Project Number: CM-TAC-0011

INHIBITION OF *S. EPIDERMIDIS* ADHESION USING SELF-ASSEMBLED MONOLAYERS

A Major Qualifying Project Report:
submitted to the Faculty
of the
WORCESTER POLYTECHNIC INSTITUTE
In partial fulfillment of the requirements for the
Degree of Bachelor of Science
by

Joshua A. Strauss
Date: August 1, 2006

Approved:

Professor Terri A. Camesano, Advisor

Preface

The primary goal of this project was to investigate the adhesion and viability of *Staphylococcus epidermidis*, a clinical isolate, on chemically modified gold surfaces known as self assembled monolayers (SAMs). The presence and viability of bacteria on the substrates were verified using dyes that can distinguish between live and dead bacterial cells. Methods such as AFM analysis and plate counting were also employed. The SAMs included 4-(16-bromo hexadecyloxy)pyridine (PYR), (1-Mercaptoundec-11-yl)tri(ethylene glycol) (TEG), 5-(10-mercaptodecyloxy)-isophthalic acid (IPA), and isophthalic acid with silver (IAG). Experiments were also conducted by first coating SAMs with a model protein, fetal bovine serum (FBS), and then conducting adhesion and viability studies.

S. epidermidis was grown in tryptic soy broth (TSB) until the mid-exponential phase. Bacteria were diluted in sterile 0.1 M MES buffer solution to a concentration of 2×10^7 cells/mL. Slides were exposed to bacteria solution for 30 minutes, followed by staining with propidium iodide and Syto 9, which allowed us to quantify the number of viable and non-viable bacteria. The attachment (retention) on and viability of cells were explored using fluorescence microscopy. The SPOT Advanced program captured and overlapped live/dead photos for analysis.

Experiments confirmed that the SAMs affected *S. epidermidis* in terms of adhesion and viability. In studies conducted without the FBS coating on the gold, PYR and TEG resulted in the greatest loss of bacterial viability. IAG and IPA, which are identical molecules except that some silver is complexed with the IAG, showed significantly different behavior in terms of bacterial viability. This was likely due to the

presence of silver ions in the IAG, as silver is a known antimicrobial agent. In the bacterial retention experiments, IPA, IAG, and TEG were most effective in terms of limiting bacterial adhesion. The low retention affinity to IPA and IAG were confirmed via AFM studies (Emerson, 2006). TEG, a commercially available product, performed comparably to IPA and IAG, signaling the need for further studies with IPA and IAG.

When FBS was introduced on the substrates, *S. epidermidis* retention was markedly reduced. Retention of bacteria onto FBS + gold was reduced by over 75% compared to bare gold. When the FBS coating was applied to the IAG and IPA SAMs, bacterial retention was reduced by >95% compared to non-protein coated substrates. This is a promising implication that SAMs can influence biofilm forming bacteria on implanted catheters, since biomaterials in the body will always become coated with indigenous proteins.

These results demonstrate that chemically modified surfaces (i.e. SAMs) can be a useful part of biomaterial design, if the goal is to develop materials that resist the retention and viability of *S. epidermidis*.

Acknowledgements

I would first like to thank my advisor, Professor Terri A. Camesano, of the Department of Chemical Engineering at WPI, for giving me the opportunity to work in the laboratory with all the wonderful graduate students. Through her guidance, I was accepted to the 106th American Society for Microbiology General Meeting and that experience was one of my highlights here at WPI.

Yatao Liu worked with me every step of the way, and for that I am deeply appreciative. His knowledge and ability as a teacher made the project very interesting and fun for me, "respectively". He is the man. I would also like to thank Eftim Milkani for providing the many substrates for us, Dr. Emerson for all of the experiments with IPA, IAG, PYR, and TEG that made this project possible (who, by the way, makes a great hummus), and Arzu Atabek for providing me literature about the AFM.

Table of Contents

List of Figures

List of Tables

1.0 - Introduction

S. epidermidis was once believed to be a harmless strain of bacteria (Gu *et al.*, 2005). Commonly found on the skin, it protects the host from more virulent skin pathogens such as *S. aureus* (Gu *et al.*, 2005). Normally *S. epidermidis* is regulated by the body's immune system. When a medically implanted device is inserted into the body, the immune system becomes vulnerable to a devastating infection (Depuydt *et al.*, 2005). *S. epidermidis* appears as a grape like structure that attaches to other bacteria held together by a 'sticky' outer membrane (Giesbrecht *et al.*, 1998). This mass of bacteria is known as the biofilm.

The same sticky outer membrane that enables *S. epidermidis* to form the biofilm also allows the bacteria to attach to catheters. The use of SAMs to chemically modify surfaces is a novel approach to altering the adhesion behavior and viability of bacteria that encounter medically implanted devices (Ulman, 1996).

This project explores how SAMs affect the retention and viability of a clinically isolated bacterium, *S. epidermidis*. The goal of this project was to quantify these effects using two nucleic acid stains that allow live and dead bacteria to be distinguished via fluorescence microscopy. The SAMs explored were 4-(16-bromo hexadecyloxy)pyridine (PYR), (1-Mercaptoundec-11-yl)tri(ethylene glycol) (TEG), 5-(10-mercaptodecyloxy)-isophthalic acid (IPA), and isophthalic acid with silver (IAG). Experiments were also conducted by coating the SAMs with a model protein, fetal bovine serum (FBS), to mimic *in vivo* conditions.

The advantages of using Syto 9 and propidium iodide are that cells are easily counted under fluorescence microscopy, there is a clear distinction between live/dead

cells, a small amount of dye is necessary per experiment, and once stained, the cells are ready for viewing in 5 minutes. Counting was carried out using the SPOT Advanced software and the results of the live/dead experiments were correlated with results obtained from AFM, contact angles, and plate counting.

2.0 - Literature Review

2.1 – Catheter Related Infections

2.1.1 – Catheter Related Blood Stream Infections (CRBSI)

Used in hospitals to readily inject drugs, blood, or plasma, catheters are vital to support ill patients (Depuydt *et al.*, 2005 and WebMD, Inc., 2005). Catheters have become so integrated in modern society that there is a strong likelihood of every single person being host to a catheter during their lifetime (Depuydt *et al.*, 2005). Despite the best efforts of hospital employees, bacteria readily infect patients with indwelling medical devices causing annual cost estimates of CRBSIs that range from $0.3-2 billion annually (Depuydt *et al.*, 2005).

It is estimated that from 1992-2002, there were ~250,000 central venous catheter infections per year (Depuydt *et al.*, 2005). Of those infected in the intensive care unit (ICU), there is a 25% mortality rate (Depuydt *et al.*, 2005). Patients either on ventilators or in the ICU can expect to spend an extra week in the hospital if an infection develops. The cost of the stay likewise increases significantly by an average of 40% (Depuydt *et al.*, 2005).

Coagulase-negative staphylococci are the organisms most associated with CRBSIs, while gram-negative bacteria are much less common. Gram-positive bacteria, including *Staphylococci* and *Enterococci*, are the most common culprits (Depuydt *et al.*, 2005).

Some startling data found many species of bacteria were highly resistant to antibiotics. For example, 94.6% of coagulase-negative bacteria are resistant to antimicrobials, while *S. aureus* is resistant 45.5% of the time (Depuydt *et al.*, 2005). Of

the 186 episodes of infection explored, only two cases involved *Sphingobacterium meningosepticum.* In both cases the bacteria were resistant to antimicrobials, which led to a life-threatening situation for the hosts. The complete list may be found in Table 2.1 (Depuydt *et al.*, 2005).

Table 2.1 - Bacteria Isolated from Nosocomial (hospital) Infections, adapted from (Depuydt *et al.*, 2005)

Microorganism	No. (%) of isolations	No. (%) of isolations of antimicrobial-resistant pathogens[a]	No. (%) of episodes in which the pathogen was isolated	No. (%) of episodes in which the bacterium was isolated as a single pathogen
Gram-positive bacteria				
All	140 (64.5)	98 (70.0)	125 (67.2)[b]	97 (52.2)
Coagulase-negative staphylococci	93 (42.9)	88 (94.6)	93 (50.0)	75 (40.3)
Staphylococcus aureus	22 (10.1)	10 (45.5)	22 (11.8)	17 (9.1)
Enterococci	23 (10.6)	0 (0)	23 (12.4)	5 (2.7)
Streptococci	2 (0.9)	0 (0)	2 (1.1)	0 (0)
Gram-negative bacteria				
All	54 (24.9)	21 (38.9)	52 (28.0)[c]	40 (21.5)
Enterobacter species	13 (6.0)	6 (46.2)	13 (7.0)	10 (5.4)
Pseudomonas aeruginosa	12 (5.5)	6 (50.0)	12 (6.5)	7 (3.8)
Serratia marcescens	9 (4.2)	2 (22.2)	9 (4.8)	7 (3.8)
Klebsiella species	8 (3.7)	1 (12.5)	8 (4.3)	6 (3.2)
Acinetobacter species	5 (2.3)	4 (80.0)	5 (2.7)	5 (2.7)
Escherichia coli	3 (1.4)	0 (0)	3 (1.6)	1 (0.5)
Proteus species	2 (0.9)	0 (0)	2 (1.1)	2 (1.1)
Sphingobacterium meningosepticum	2 (0.9)	2 (100)	2 (1.1)	2 (1.1)
Candida species	21 (9.7)	2 (9.5)	21 (11.3)	17 (9.1)
Anaerobic bacteria	2 (0.9)	0 (0)	2 (1.1)	1 (0.5)
2 Microorganisms	...	...	31 (16.7)	...
Total	217 (100)	121 (55.8)	186 (100)	155 (83.3)

2.1.2 The Biofilm

Bacteria may be found in two separate forms; planktonic (i.e. free in suspension), and as part of biofilm. In nature, 99.9% of bacteria are found within biofilms (Depuydt *et al.*, 2005). Biofilms are commonly thought of as 3-dimensional matrices consisting of 75% to 95% 'slime' with the remainder being the cells (Giesbrecht *et al.*, 1998). There are, however, exceptions for certain bacteria that grow in 1 or 2 dimensional manners. The slime is most important for the survival of the bacteria, and in certain cases toxic for the host. The slime acts as a shield against antibiotics, environmental stresses, and bodily

defenses, making it the pristine environment for bacteria to thrive (Giesbrecht *et al.*, 1998).

The 'slime' is different for each type of bacterium, consisting largely of charged and neutral polysaccharide groups (Giesbrecht *et al.*, 1998). The polysaccharides give the 'slime' its sticky characteristics that attach cells to substrates and each other. Indwelling charges are important for ion exchange between cells in the biofilm (Edtrom Industries, Inc., 2005). This is important for trapping and distributing food such as iron within the biofilm so that the cells do not starve. In some environments, such as water distribution systems, cells have demonstrated an amazing ability to survive given a limited nutrient environment of only trace amounts of iron and other organic compounds (Edtrom Industries, Inc., 2005).

The vast majority of bacteria live in biofilms that have a lifecycle of five stages. Whether it is in industrial piping or in catheter, the life cycle is remarkably similar (Edtrom Industries, Inc., 2005).

The first step in biofilm formation is known as surface conditioning. In the body, free plasma proteins in the blood attach onto the catheter surface (Ryder, 2005). Fibronectin, laminin, fibrin, collagen, and immunoglobulins are all known to attach to implants (Ryder, 2005 and Leid *et al.* 2002). Soon after, the coagulation alerts platelets and polymorphonuclear leukocytes to attach to the implant (Leid *et al.* 2002). This is followed by planktonic bacteria utilizing their extracellular polymeric substances to permanently adhere to the surface. The physicochemical forces involved in adhesion include polarity, electrostatics, van der Waal's forces, and hydrophobic interactions, which will be discussed in later sections (van Loosdrecht *et al.*, 1987). Once coating by

bodily proteins occurs, surface properties are altered, making it easier for certain bacteria to adhere.

Two main molecular groups, polymeric carbohydrates and polymeric proteins, have been shown to promote bacterial retention to substrates. In the case of *S. epidermidis,* two prominent polysaccharides have been identified including capsular polysaccharide (PSA) and polysaccharide intercellular adhesion (PIA) (Morales *et al.*, 2004). The accessory gene regulator (*agr*) system influences both biofilm dispersal and attachment of cells to surfaces, but does not regulate PIA expression (Morales *et al.*, 2004). Studies have shown that disrupting the *agr* locus of *S. epidermidis* results in higher adhesion to polystyrene, increased biofilm formation, and increased expression of the AtlE gene that enhances attachment to abiotic surfaces (Morales *et al.*, 2004).

For certain bacteria such as *Pseudomonas aeruginosa*, plasma proteins present on abiotic surfaces promote retention (Murga *et al.*, 2001). *S. aureus* binds better with the body's proteins, but inhibits retention of *S. epidermidis* and gram-negative bacteria (Murga *et al.*, 2001). The mechanisms behind bacteria binding to substrates are far from understood.

Once attachment occurs, phenotypic changes alter protein expression within the cell in a matter of seconds; thus initiating the biofilm, regardless of the type of bacteria (Ryder, 2005 and Morales *et al.*, 2004). The proteins irreversibly anchor the bacteria to the surface. Within 12 minutes cells begin accumulating proteins and polysaccharides known as 'slime' that further bond the cells to the substrate and to other cells within the matrix (Morales *et al.*, 2004). The biofilm grows in an upwards motion as daughter cells are created through further division.

Although this three-dimensional structure for biofilm formation is very common, certain bacteria grow in colonies that are not of the 3-D type. *Streptococcus,* for example, grows in long chains (Giesbrecht *et al.* 1998). Bacteria including *Peiococcus, Thiopedia, Lampropedia, and Deinococcus* grow in 2 dimensional matrices (Giesbrecht *et al.* 1998). These bacteria represent an exception to the commonly understood definition of a biofilm, because daughter cells do not break off the biofilm in an upward motion.

Eventually, the biofilm may grow as high as 60 μm before shear stresses in the bloodstream break off sections of the biofilm (Ryder, 2005). Planktonic bacteria spread to other locations on the implanted device or in the host (Ryder, 2005). It is also suspected that cell to cell signaling may provoke this detachment in order to keep cells at the bottom of the biofilm from starving (Ryder, 2005).

Normally the body's immune system destroys bacteria before they are allowed to construct a biofilm. In the cases when bacterial retention is promoted, such as when a catheter is inserted into the body, bacteria pose a serious threat that the immune system cannot easily fight (Morales *et al.*, 2004). Antibiotics are not always effective against biofilms, since bacteria penetrate deep into bodily tissues (Morales *et al.*, 2004). Bacteria are found both in and around the inserted catheters (Morales *et al.*, 2004). Scientists have studied much about planktonic bacteria, but have only begun to understand bacteria in biofilms (Morales *et al.*, 2004).

Recent studies with *S. aureus* demonstrate that the body's immune system has defenses against biofilms. However, these defenses are not nearly as effective against *S. aureus* in biofilm as they are against planktonic bacteria. It has been observed that

leukocytes, also known as white blood cells, imbed and attach to biofilms (Morales *et al.*, 2004). For reasons unknown, there appears to be a "leukocyte halo" inside the biofilm where some *S. aureus* are dead (Morales *et al.*, 2004). This suggests that some kind of deactivation occurs of the body's immune system. Further, these results give rise to the hope that antibiotics may once again play a pivotal role in biofilm treatment. (Morales *et al.*, 2004).

Since biofilm-associated infections are very difficult to treat, prevention is the best way to fight these potentially deadly organisms. Before development of products that are anti-pathogenic, methods need to be devised that can measure the effectiveness against bacteria.

2.2 – Fluorescence Microscopy

2.2.1 – Bacteria Viability Tests

Intact DNA was long associated with viable bacteria until recently (Kloos and Bannerman, 1994). The polymerase chain reaction (PCR) has been found to be detectable in the DNA of non-culturable bacteria (Kloos and Bannerman, 1994). Other tests have been developed to ascertain the state of bacteria, including testing cellular integrity and metabolic activity (Kloos and Bannerman, 1994 and Boulus *et al.*, 1999).

The goal of the live/dead test is to determine if the cells are viable and can be pathogenic. There are a plethora of causes for viability loss including UV radiation, malnutrition, toxins, osmotic shock, pH changes, temperature, and oxygen concentration (Kloos and Bannerman, 1994). Studies have shown that non-culturable cells in the laboratory setting have difficulty growing *in vivo* (Kloos and Bannerman, 1994). Experiments with Viable but Non-Culturable (VBNC) *Salmonella* and *Legionella pneumphila* both failed to cause infection in one study (Kloos and Bannerman, 1994).

Once resuscitated, however, the cells were able to grow and infect a host. Researchers have demonstrated that *Ralstonia solanacearum*, a plant pathogen, was able to form an infection following resuscitation (Kloos and Bannerman, 1994).

The significance of these studies is that bacteria demonstrate a lack of need for metabolic activity to remain a menace for a potential host. Other methods have developed for detecting pathogenic bacteria, which is significant for anyone concerned about public health. Methods for testing cell viability include detection of respiratory activity, environmental responsiveness, substrate responsiveness, culturability, and membrane integrity (Kloos and Bannerman, 1994, Boulus *et al.*, 1999, and Banning *et al.*, 2002)

2.2.2 – GFP, Syto 9™, and Propidium Iodide

Measuring membrane integrity is just one of many methods that can be employed to determine cell viability. Green fluorescent protein (GFP), propidium iodide, and Syto are some of the available markers used for determining cell viability. GFP, derived from the jellyfish *Aequoria*, is best used as a cell marker for counting the total number of Prokaryotic or Eukaryotic cells present (Boulus *et al.*, 1999). The downside to using GFP comes from its stability, as it can still be detected long after the cell's death. GFP is heat and UV light sensitive, thus if cells are killed by either method, they will be undetectable by GFP. Much of the same can be said for the live/dead kit composed of Syto 9 and propidium iodide. Syto 9 is a nucleic acid-binding molecule that penetrates all cell membranes and can be used to determine total cell counts (Boulus *et al.*, 1999). It too is light and heat sensitive, and if cell death occurs by exposure to excess of either, the cells will no longer be detectable. Propidium iodide cannot normally pass through cell

membranes, and can be used in conjunction with Syto 9 to determine cell viability (Boulus *et al.*, 1999).

Propidium iodide is a selective molecule that also stains nucleic acid but can only pass through compromised cell walls. The molecule is highly charged compared to Syto 9, such that if a cell is visible under the FITC filter and invisible under the Texas Red filter, the cell membrane is intact and the cell is likely viable (Boulus *et al.*, 1999). On the other hand, if the cell appears red under the Texas Red filter, cell membrane integrity is compromised to the extent that normal cell functions cannot continue and the cell is considered dead (Boulus *et al.*, 1999).

2.2.3 – Staining for Water Quality

Nucleic acid stains such as acridine orange and the live/dead test from the *Bac*Light™ kit have been widely used to detect the presence of bacteria. From an environmental perspective, one of the most exciting uses is measuring the efficiency of the disinfection process in water treatment plants. In Montreal, Canada at the Atwater treatment plant, a study focused on two strains of *Escherichia coli*, ATCC 11229 and an environmental isolate, and *Citrobacter freundii*. All were studied to measure the effectiveness of the kit in detecting the viability and quantity of bacteria, along with assessing the overall plant operation. The results of the live/dead *Bac*Light total (BLT) counts were validated against other proven methods of detection, including AODC (acridine orange direct counts), CTC (5-cyano-2,3-ditolyl tetrazolium), DAPI (4,6-di-amidino-2-phenylindole), m-Endo agar, and m-T17 agar colony counts (Boulus *et al.*, 1999).

When checking for the total cells present, the *Bac*Light kit results were nearly identical to the AODC, CTC1 + Syto, and CTC2 + DAPI tests. From these data, there is no clear advantage of using one test over another. The standard deviations were low for each test, indicating a high degree of reliability (Figure 2.1).

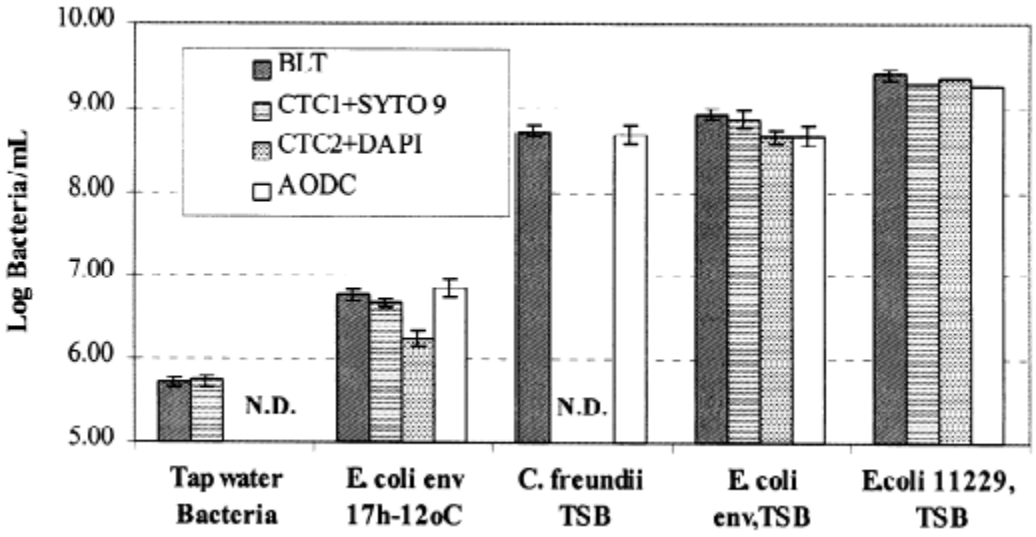

Figure 2.1 - Total Cell Counts with Various Stains, adapted from (Boulus *et al.*, 1999)

Cells were also immersed in increasing concentrations of chlorine to observe changes in viability. The *Bac*Light kit detected an increase in total dead cells, which is consistent with an increase in chlorine concentration. (Figure 2.2)

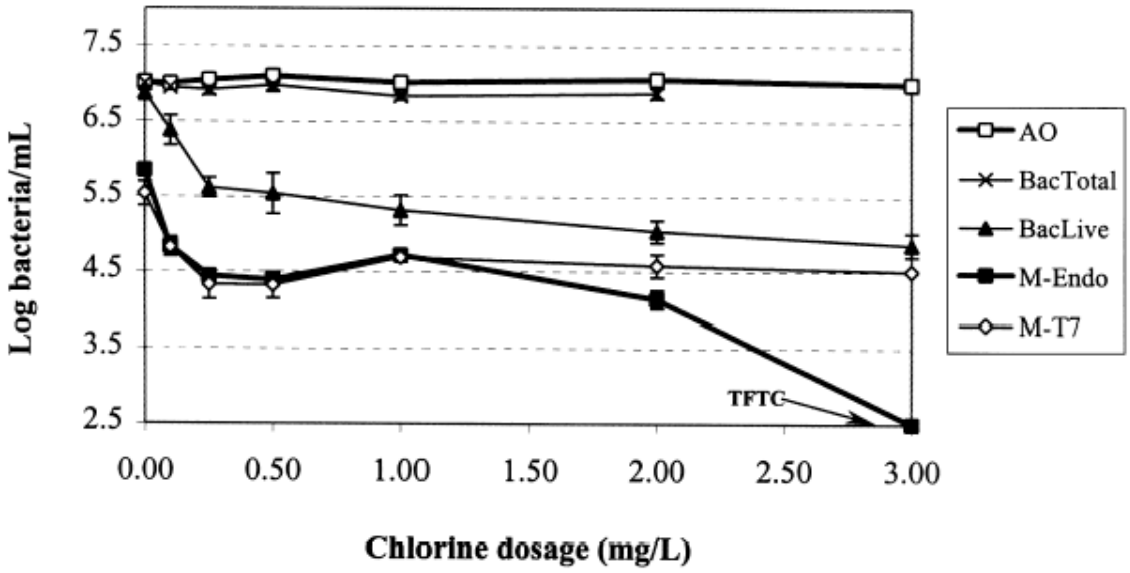

Figure 2.2 - Live/Dead Tests, adapted from (Boulus *et al.*, 1999)

The *Bac*Light kit has many advantages over other methods of testing for viability. Foremost is rapid use. Following application, cells are stained in a matter of minutes. During this procedure, there is a significant contrast between total cell counts, which appear green, and dead cells, which appear red (Boulus *et al.*, 1999 and Banning *et al.*, 2002). Noteworthy about this kit is that of all viability tests, the *Bac*Light detected the highest number of viable cells. The results of using the kit should therefore be verified using other methods to ensure reliable data (Boulus *et al.*, 1999 and Banning *et al.*, 2002).

With many methods to track the presence and status of bacteria, it is also very important to understand the mechanisms behind bacterial adhesion to develop effective anti-microbials.

2.3 Bacterial Retention

2.3.1 – Bacterial Capsules

For bacteria, a very important factor for retention is the capsule. Found in both gram positive and negative cells, the capsule exists outside the cell wall, eclipsing the bacterium (Boulus *et al.*, 1999). The capsule is made of proteins and polysaccharides that make retention to substrates possible for the bacteria (Boulus *et al.*, 1999). An important discovery regarding *S. epidermidis* is that if the capsule is more hydrophobic, the binding forces between cell and polymer (hydrophobic) surfaces are generally stronger (Boulus *et al.*, 1999). *S. haemolyticus,* which has similar degrees of cell wall hydrophobicity and charge, binds better to plasma proteins than *S. epidermidis*. There are other important factors that allow bacteria to adhere to surfaces than hydrophobicity, such as the fimbiae and flagella (An and Friedman, 1997).

2.3.2 – Fimbriae or Pili and Flagella

Fimbriae are either string or rod shaped structures composed of protein subunits called pilin, which form polymers making up multiple units of fimbriae. The fimbriae usually have a maximum diameter up to 7 nm, and their lengths range from 0.2 to 20 nm. Fimbriae are most commonly found on gram-negative bacteria, where 100-1000 fimbriae may be present on the surface of a bacterium. The importance of fimbriae may be found in the fact that gram-negative bacteria are more virulent than nonfimbrial species (An and Friedman, 1997).

The flagellum is an organelle also found on the exterior of certain bacteria that assists in motility. The flagellum operates by spinning at 200 to 1000 rates per minute (rpm) (Prescott *et al.,* 2005). Flagella are threadlike protein structures that measure ~20

nm across and 15-20 μm long (Prescott *et al.,* 2005). Bacteria with flagella usually move toward chemical attractants through a process called chemotaxis (Prescott *et al.,* 2005). Bacteria can detect sugar concentrations as low as 10^{-8} M and use the process to move towards the food source (Prescott *et al.,* 2005). Flagella may also assist bacteria to attach to surfaces by reaching out and binding to the substrate (Prescott *et al.,* 2005).

2.3.3 – Substrate Dynamics

Thermodynamics may be employed to understand the microscopic forces that promote bacterial retention to substrates. To understand the thermodynamics of bacterial retention, some assumptions need to be made. Bacterial adhesion will be considered favorable if the surface free energy decreases due to attachment (Absolom *et al.*, 1983). Likewise, adhesion will not be considered favorable if surface free energy increases. Neglecting electric and biochemical interactions, the change in surface free energy for a given area may be expressed as (Absolom *et al.*, 1983)

$$\Delta F^{adh} = \gamma BS - \gamma BL - \gamma SL \qquad (1)$$

where F^{adh} is the free energy of adhesion, γBS is the bacterium-substratum interfacial tension, γBL is the bacterium-liquid interfacial tension, and γSL is the substratum-liquid interfacial tension. Young's equation expands on the above free energy balance and can be used to obtain data on interfacial tensions of solid surfaces with the relation (Absolom *et al.*, 1983)

$$\gamma sv - \gamma sl = \gamma lv \times \cos\theta \qquad (2)$$

where γsv is the interfacial tension between a solid substratum and vapor, γsl between the solid substratum and liquid, γlv between the liquid and vapor, and θ is the contact angle of the liquid resting on the solid. Since γsl is a function of both γsv and γlv, using

experimentally derived contact angle data and surface free energy data and combining with Young's equation, the relationship yields (Absolom *et al.*, 1983)

$$\cos\theta = \frac{(0.015\gamma sv - 2.00) \times \sqrt{\gamma sv \times \gamma lv} + \gamma lv}{\gamma lv(0.015\sqrt{\gamma sv \times \gamma lv} - 1)} \quad (3)$$

The purpose of thermodynamics studies is to determine how bacterial adhesion varies when different types of substrates are each considered. γBV (bacterial surface tension compared to vapor tension) relates to the tension of the liquid medium (γlv) in three ways (Absolom *et al.*, 1983)

$$\gamma lv < \gamma BV \quad (4)$$

$$\gamma lv > \gamma BV \quad (5)$$

$$\gamma lv = \gamma BV \quad (6)$$

In the case of equation 4, ΔF^{adh} decreases, and we would expect an increase in the number of bacteria adhering to a substrate. In equation 5, the opposite would be true. This scenario would represent a decrease in the number of adhering bacteria. In the case of equation 6, bacterial adhesion is independent of surface tension (Absolom *et al.*, 1983).

In a study comparing 5 strains of bacteria, thermodynamics alone predicted the adherence of bacteria to substrates including sulfonated polystyrene, acetal resin, polyethylene, polystyrene, and fluorinated ethylene-propylene copolymer during the initial stages of experimentation (Absolom *et al.*, 1983). An unexpected result occurred during the experiment when bacteria adhered to the substrates despite $\Delta F^{adh}>0$. The authors suggested that this phenomenon may have been due to electrostatic interactions between the substrate and bacteria. When the ionic strength of the liquid was very low,

bacterial adhesion was virtually non-existent due to increased electrostatic repulsion (Absolom *et al.*, 1983).

In calculating a substrate's surface free energy, contact angles are measured with water, water n-propanol mixtures, or α-bromonaphthalene, which vary in terms of polarity. Surface free energy can be calculated with the following equation (Busscher *et al.*, 1984)

$$\cos\theta = -1 + 2\times(\gamma_s^d \times \gamma_l^d)^{0.5} \times \gamma_l^{-1} + 2\times(\gamma_s^p \times \gamma_l^p)^{0.5} \times \gamma_l^{-1} - \pi_e \times \gamma_l^{-1} \quad (7)$$

where *d* is the dispersion component, *p* is the polar component, γ_s is the surface free energy of the solid, γ_l is the surface free energy of the liquid, and π_e represents the spreading pressure. Equation 7 generates a least squares regression analysis useful for multiple measured angles to obtain the surface free energy (Busscher *et al.*, 1984).

A more common set of liquids that can be used to measure contact angles to calculate the surface free energy includes water (Θ_w), formamide (Θ_f), and diiodomethane (Θ_d). Surface tensions can be calculated via the Young-Dupré equation (Gallardo-Moreno *et al.*, 2004)

$$\gamma_L(\cos\theta_L + 1) = 2\sqrt{\gamma_B^{LW} \times \gamma_L^{LW}} + 2\sqrt{\gamma_B^{+} \times \gamma_L^{-}} + 2\sqrt{\gamma_B^{-} \times \gamma_L^{+}} \quad (8)$$

where γ^- and γ^+ are the electron donor and electron acceptor parameters, *B* is bacterium, *L* is liquid and

$$\gamma_L^{LW} + \gamma_L^{AB}\ \gamma_L^{LW} + \gamma_L^{AB} \quad (9)$$

is the surface tension of the probe in the liquid (Gallardo-Moreno *et al.*, 2004).

To calculate the total interaction energy between the bacterium and substrata in water (ΔG_{adh}^{Total}), the forces between dipole-dipole, dipole-induced dipole, and induced dipole-induced dipole LW long-range interactions are expressed in a single term and the

acid-base short range force characteristics as a separate term yielding (Gallardo-Moreno *et al.*, 2002)

$$\Delta G_{adh}^{Total} = \Delta G_{adh}^{LW} + \Delta G_{adh}^{AB} \quad (10)$$

where

$$\Delta G_{adh}^{LW} = (\sqrt{\gamma_B^{LW}} - \sqrt{\gamma_S^{LW}})^2 - (\sqrt{\gamma_B^{LW}} - \sqrt{\gamma_W^{LW}})^2 - (\sqrt{\gamma_S^{LW}} - \sqrt{\gamma_W^{LW}})^2 \quad (11)$$

and

$$\Delta G_{adh}^{AB} = 2(\sqrt{\gamma_W^+}(\sqrt{\gamma_B^-} + \sqrt{\gamma_S^-} + \sqrt{\gamma_W^-}) + \sqrt{\gamma_W^-}(\sqrt{\gamma_B^+} + \sqrt{\gamma_S^+} + \sqrt{\gamma_W^+}) - \sqrt{\gamma_B^-\gamma_S^+} - \sqrt{\gamma_B^+\gamma_S^-}) \quad (12)$$

Another method for determining (ΔG_{adh}^{Total}) can be to measure the free energy between bacteria [1], substratum [2], and medium the substratum is immersed in [3], and $\gamma_{3,}$ which is the surface tension of the water that is expressed as $\Delta G_{1,2,3}$. The sum of the interactions is (Gallardo-Moreno *et al.*, 2002)

$$\Delta G_{1,2,3} = \Delta G_{1,2} - \Delta G_{1,3} - \Delta G_{2,3} - 2\gamma_3 \quad (13)$$

To calculate the free energy between bacterium, substratum, and immersion liquid, $\Delta G_{ij,}$ where *i* and *j* represent [1], [2], or [3], the following equation can be used (Gallardo-Moreno, *et al.*, 2002)

$$\Delta G_{ij} = \gamma_{ij} - \gamma_i - \gamma_j = -2(\sqrt{\gamma_i^{LW} \times \gamma_j^{LW}} + \sqrt{\gamma_i^- \times \gamma_j^+} + \sqrt{\gamma_i^+ \times \gamma_j^-}) \quad (14)$$

While the thermodynamic model is preferable for some researchers of bacterial surface retention, DLVO theory is an alternative method.

2.3.4 – DLVO Theory

DLVO stands for the originators of the theory; Derjaguin, Landau, Verwey, and Overbeek (Israelachvili, 1992). DLVO theory is based on molecular interaction profiles by summing electrostatic and van der Waals interactions (Israelachvili, 1992).

Electrostatic forces arise from the Double Layer Theory. When an object is placed into solution, its surface becomes charged. If the object, for example, is associated with oxygen molecules on the surface, then hydrogen atoms in the water will be attracted to the charged molecules (Israelachvili, 1992). Usually a small amount of the oxygen molecules will interact with the hydrogen molecules, leaving a net negative charge on the substrate. The net negative charge attracts positively charged ions in the solution that would normally have been dissociated (Israelachvili, 1992). The double layer theory is applied to bacterial adhesion by correlating electrostatic potential produced by charges to the ion density in a bacterium's cytoplasm (Israelachvili, 1992).

London dispersion forces, or van der Waals forces, are associated with the polarization of molecules into dipoles (Israelachvili, 1992). Originally, van der Waals forces were considered the only intermolecular forces, but thus neglected specific interactions forces, solvation forces and depletion forces (Israelachvili, 1992). Between two spheres, the van der Waals interaction may be expressed as follows (Israelachvili, 1992)

$$F_v = -\frac{A_{132} a_m a_p}{6h^2(a_m + a_p)} \tag{15}$$

where h is the separation distance, evaluated as H_0, the theoretical closest distance 1.57 Å, A_{132} is the Hamaker constant, a_m is the radius of the bacteria, and a_p is the radius of the tip.

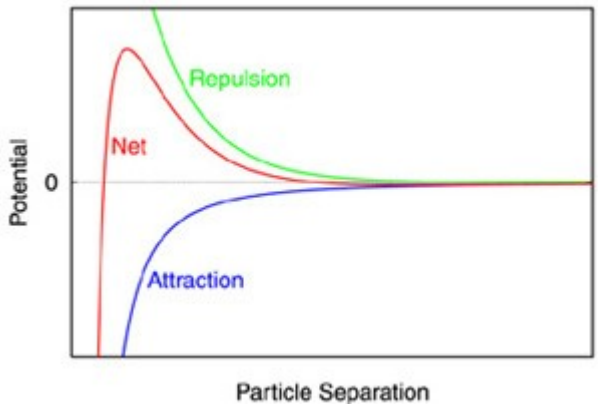

Figure 2.3 – DLVO interactions between two spheres. Blue curve represents van der Waals potential (attraction), green curve represents electrostatic potential (repulsion), and the red curve is the net potential. The energy barrier is when the net potential reaches a maximum. As the distance between objects increases, DLVO potential approaches zero. Adapted from (Gudehus, 2006).

A modification to the DLVO theory incorporates the hydrophobic effects, also known as the acid-base interactions. DLVOX and DLVO-AB are exactly the same since hydrophilic substrates tend to be more acidic and hydrophobic substrates have a tendency towards being basic (Gudehus, 2006). In some cases, bacterial retention to a substrate is better modeled using the modified DLVOX theory as opposed to the DLVO, but both ignore important factors such as surface roughness and nanoscale molecular forces on the substrates (Israelachvili, 1992).

2.3.5 –Gouy-Chapman Model of Electrostatic Interactions

The Gouy-Chapman theory suggests a correlation between charge density and electrical potential of a substrate to the concentration of ions in a surrounding solution. This is especially important in measuring ions in solution that may impact the viability or adhesion of bacteria. According to the Nernst equation, activity of a solution may be measured in equilibrium partitioning between two phases (0 and ∞) (Schmitt *et al.*, 1998)

$$\alpha_{10} = \alpha_{\infty} \exp(-ZFE_{0\to\infty}/RT) = C_{\infty}\Gamma_{\infty} \exp(-Z_i FE_{0\to\infty}/RT) \quad (16)$$

where α is the chemical activity of the ion, C is the ion concentration, E is the electric potential, Γ is the activity coefficient of the ion, Z is the charge on the ion, E is the electrical potential difference between phases *0* and ∞, R is the gas constant, T is the temperature, and F is the Faraday constant (Schmitt *et al.*, 1998).

If the concentration of the ions can be computed in phase 0, then the activity coefficient may also be determined (Schmitt *et al.*, 1998)

$$C_{i0} = (C_{i\infty}\Gamma_{\infty}/\Gamma_{i0}) \exp(-Z_i FE_{0\to\infty}/RT) \quad (17)$$

where the variables correspond to phase ∞.

The Gouy-Chapman theory was established to form a relationship between solutions and charged surfaces and is expressed in the Grahame equation (Schmitt *et al.*, 1998)

$$\sigma^2 = (0.00345)\sum_i C_{i\infty}(\exp(-Z_i E_0/25.7) - 1) \quad (18)$$

where σ is the density of charged particles, E_o is the electrical potential, and $C_{i\infty}$ is the ion concentration at infinite distance from the substrate (Schmitt *et al.*, 1998).

The Poisson-Boltzmann equation yields the potential, electric field, and counterion density at any point between two substrates. The PB equation is expressed as (Israelachvili, 1992)

$$d^2\Psi/dx^2 = -ze\rho/\varepsilon\varepsilon_0 = -(ze\rho_0/\varepsilon\varepsilon_0)e^{-xe\Psi/kT} \quad (19)$$

where Ψ is the potential, ρ is the number density of ions of valency z, k is the Boltzmann's constant, T is the temperature, ε_0 is the permittivity of free space, and $-e$ is the electronic charge.

Substituting the Grahame equation into the Poisson-Boltzmann equation yields (Schmitt *et al.*, 1998)

$$d^3E_x/(dx^2) = -1/(\varepsilon_1\varepsilon_0)\sum_i Z_i F C_{i\infty} \exp(-Z_i F E_0/RT) \quad (20)$$

This equation is useful for calculating the electric potential of a solution and the external concentrations when α is a low value (Israelachvili, 1992).

Stern made a modification to the Gouy-Chapman theory by taking into account changes in α due to ion binding onto the substrate surface. This relationship between surface ligand *Q"* and an ion *S'* is expressed in the following form (Schmitt *et al.*, 1998)

$$[QS^{X+Y}] = K_{QS}[Q''][S']_0 \quad (21)$$

where *Q"* and $[QS^{x+y}]$ are ion concentrations, S'_0 is the ion concentration at the surface, K_{QS} is an association constant, and *x* and *y* are charges (Schmitt *et al.*, 1998).

Gouy and Chapman combined both the Poisson equation, which describes the attraction of counterions to a surface, and the Boltzmann relation, which describes the repulsion of counterions in an area of high concentration. In the case with low surface potential, $\Psi(0)$, the following statement can be made (Israelachvili, 1992)

$$\Psi(0) = \sigma/(\varepsilon_a\varepsilon_0\kappa) \quad (22)$$

where ε_a is the dielectric constant, ε_0 is the permittivity of free space, σ is the surface charge density, and κ is the inverse Debye length $([(\varepsilon_0\varepsilon_a kT)/(2z^2e^2c)]^{0.5})$. Across a distance, *x*, the potential varies as follows (Israelachvili, 1992)

$$\Psi(x) = \Psi(0)\exp(-\kappa x) \quad (23)$$

The surface potential, $\Psi(0)$, is predicted by the Gouy equation and is directly related to the concentration of ions in solution, c, and the surface charge density, σ, by: (Israelachvili, 1992)

$$\sinh[ze\Psi(0)/2kT] = A\sigma/(c)^{0/5} = (8\varepsilon_a\varepsilon_0 kT)^{-0.5}\sigma/(c)^{0.5} \quad (24)$$

When the potential is larger than 25 mV, Gouy-Chapman theory predicts the rate at which the potential drops increases near the substrate as follows (Israelachvili, 1992)

$$\Psi(x) = \frac{(2kT)}{e}\ln\left(\frac{\exp[\frac{e\Psi(0)}{2kT}]-1}{\exp[\frac{e\Psi(0)}{2kT}]+1}\right)\ln\frac{[1+\alpha\exp(-\kappa x)]}{[1-\alpha\exp(-\kappa x)]} \quad (25)$$

By having an understanding of the mechanics that lead to colloidal interactions, it is possible to predict what certain substrate modifications will have on bacterial retention.

2.4 – Surface Modifications

2.4.1 – *S. epidermidis* Retention

S. epidermidis is a gram-positive bacterium that is commonly found on the skin. It forms grape-like structures that compose a biofilm (Prescott *et al.,* 2005). *S. epidermidis* has been shown to commonly colonize polymer implants, whereas *S. aureus* is more commonly found on metallic implants (Giesbrecht *et al.*, 1998). In patients and laboratory settings, the number of bacteria adhering to a catheter varies according to the strain of bacteria and type of material (An and Friedman, 1997).

Many studies have been conducted to try limiting the number of bacteria adhering by altering the surface chemistry composition (Salerno, 2005 and Mermel, 2001). Some substrates found to limit bacterial adhesion include peptide coatings, pluronic surfactant coating, and amine-containing organosilicon (An and Friedman, 1997). Many more

studies have investigated other coatings that are potential candidates against biofilm forming bacteria.

2.4.2 - Chlorhexidine-Silver

Chlorhexidine-silver sulfadiazine-impregnated catheters were studied to see if they would serve as an effective anti-septic against *S. epidermidis*. Like most antibiotics, these compounds work by damaging the cell wall and ceasing mitosis. Although results were promising, disadvantages of using these compounds arose following commercialization (Schmitt *et al.*, 1998). For example, the active ingredients were only effective on the extraluminal surface, limiting the ability to kill bacteria on other regions of the catheter. Regardless, clinical studies show high levels of potency in clinical studies. Lumen intravenous catheters were coated with the compounds and the results were compared to bare catheters (Mermel, 2001).

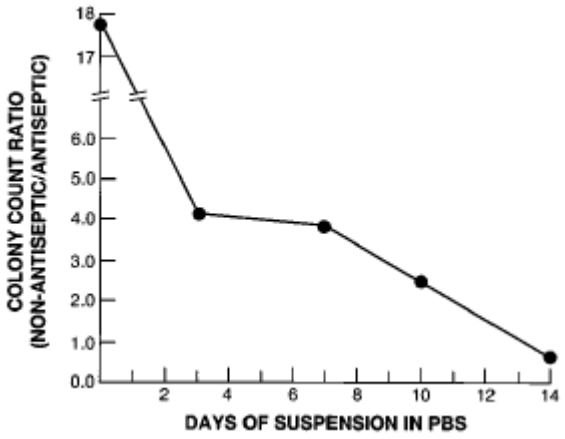

Figure 2.4 -Bare Catheter vs. Coated Catheter, adapted from (Schmitt *et al.*, 1998)

A variety of methods were used to count the number of colonies forming, including sonication and roll-plating. Via the sonication method, it was found that there

was a tenfold decrease in the number of detectable *S. epidermidis* colonies when compared to the bare catheter. After 24 hours no colonies were present. The roll-plating method yielded similar results but found a reduction that was one-twelfth the number of colonies in 1-3 hours when compared to the bare catheter (Schmitt *et al.*, 1998).

As for the duration, Figure 2.4 shows that after 14 days, the number of colonies found on the bare catheter were equal to that on the coated catheter. This may be due to the bacteria becoming immune to the antibiotics over time. Also, the PBS likely dissolved the antibiotics into solution; diluting them to the point they were no longer antiseptic (Schmitt *et al.*, 1998).

Since the time of the study, this combination of antibiotics has been commercialized for short-term intravenous catheters (Turgut *et al.*, 2005). Results in humans have demonstrated some problems. The Japanese have banned coating catheters with this 'cocktail' because multiple patients have developed serious anaphylactic reactions (Mermel, 2001). An anaphylactic reaction is an allergic reaction caused by reexposure to an antigen (Mermel, 2001). In the United States, at least one person had been diagnosed with similar symptoms as of year 2000 (Mermel, 2001).

In addition, bacteria have already been developing immunity to chlorhexidine-silver sulfadiazine. *In vitro* studies have demonstrated that *Pseudomonas stutzeri*, when exposed to gradually increasing levels of the antibiotic, became resistant (Mermel, 2001). Therefore, it is likely to expect that other bacteria can develop immunity and thus other coatings need to be explored.

2.4.3 - Minocycline-Rifampin Impregnated Catheters

A catheter coating that is more effective than chlorhexidine-silver sulfadiazine, minocycline-rifampin, is a dual antibiotic combination widely used (Mermel, 2001). The two compounds have been found to work on the extraluminal and intraluminal surfaces of a catheter. Human patients who developed infections with methicillin resistant *S. aureus* (MRSA) were prescribed a minocycline-rifampin regimen that resulted in a 95% recovery rate (Darouiche *et al.*, 1991). Researchers postulated that the same antibiotic 'cocktail' could prevent biofilm formation by impregnating the catheter with minocycline-rifampin before inserting into the patient. Despite the potency of minocycline-rifampin, this antibiotic mixture has some downfalls similar to chlorhexidine-silver sulfadiazine.

There have been no serious side effects reported to be associated with these antibiotics, but both longevity and bacterial resistance are serious issues (Mermel, 2001). Over a 7-day period, animal studies have shown that the antibiotics gradually wear off and *S. aureus* can adhere and grow biofilms (Sampath, 1999). Lab animals with the antibiotic impregnated catheters were injected with *S. aureus* at the site of the catheter. The catheters removed from these animals were placed on agar plates and *S. aureus* colonies began to form; indicating the bacteria were immune to the antibiotics. Unfortunately the idea of using multiple antibiotics to kill bacteria in a catheter may not work well since bacteria are continuously developing immunity.

2.4.4 - Taurolidine and Citrate

A study focused on preventing infections caused by *S. aureus*, which is one of the more virulent strains of bacteria, by coating catheters with a Taurolidine and Citrate

mixture (Shah *et al.*, 2002). Unlike coagulase-negative bacteria, such as *S. epidermidis*, *S. aureus* readily binds to plasma proteins (Murga *et al.*, 2001). The body's fibronectin and laminin quickly attach to the inserted device and create a pristine environment for *S. aureus*. It is suspected that *S. aureus* enters the body from contaminated medical devices and comprises 10% of CRBSIs (Depuydt *et al.*, 2005). Since *S. aureus* readily attaches to plasma proteins, it creates a dangerous situation for the host. The infection can spread to other areas of the body and sometimes leads to thrombosis, which is a blood clot in a deep vain (Foster, 2005).

At fault for this danger are a variety of toxins and proteins exhibited on the outer cell wall. Research has shown that a specific protein, known as 'Protein A', binds to IgG proteins and is the mechanism for thrombosis (Foster, 2005). *S. aureus* mutants lacking 'Protein A' that were implanted in rats demonstrated a significantly reduced degree of virulence (Foster, 2005).

The study with Taurolidine (2 H-1,2,4-thiadiazine-4,4'-methylenebis(tetrahydro-1,1',1'tetraoxid)) and Citrate had two objectives, both targeting 'Protein A' (Shah *et al.*, 2002). Primarily, the researchers wanted to reduce the incidence of thrombosis, and secondly prevent *S. aureus*, along with other bacteria, from binding to intravenous catheters (Shah *et al.*, 2002).

A commonly used chemical to prevent thrombosis is heparin. Heparin is found in bovine lung tissue and is standardized for medicinal purposes (Shah *et al.*, 2002). Made up of several sugars (Table 2.2), it creates a structure of glycosaminoglycans that catalyze the reaction of antithrombin and thrombin by one thousand times (Shah *et al.*, 2002). Although commonly known as an anticoagulant, studies have shown that doses of

heparin below 1.0 IU/mL enhance platelet activity (Shah *et al.*, 2002). Therefore, researches decided it would be advantageous to explore possibilities of replacing heparin altogether in the presence of biofilms.

Table 2.2 – Main Sugar Molecules of heparin, adapted from (RxList, Inc., 2005)

A-L-iduronic acid 2-sulfate
2-deoxy-2-sulfamino-α-D-glucose 6-sulfate
ß-D-glucuronic acid
2-acetamido-2-deoxy-α-D-glucose
α-L- iduronic acid

Citrate is an anticoagulant of the blood and platelets. Taurolidine is a promising catheter coating because it is anti-adhesive, nontoxic for mammalian cells, and an antibiotic (Mermel, 2001 and Shah *et al.,* 2002). Researchers postulate that the methylol group binds irreversibly to the walls of bacteria and exerts bactercidal (suicidal) actions (Shah *et al.*, 2002). Although no bacteria are known to be resistant to this antibiotic, bacteria are constantly evolving and may eventually be able to resist any form of antibiotic.

Shah *et al.* explored the effects that these two coatings would have against planktonic bacteria. Several log reductions of viable cells on surfaces coated with the taurolidine and citrate versus heparin were observed for *S. aureus*, as well as other Gram-negative and Gram-positive bacteria, and a fungal strain (Figure 2.5).

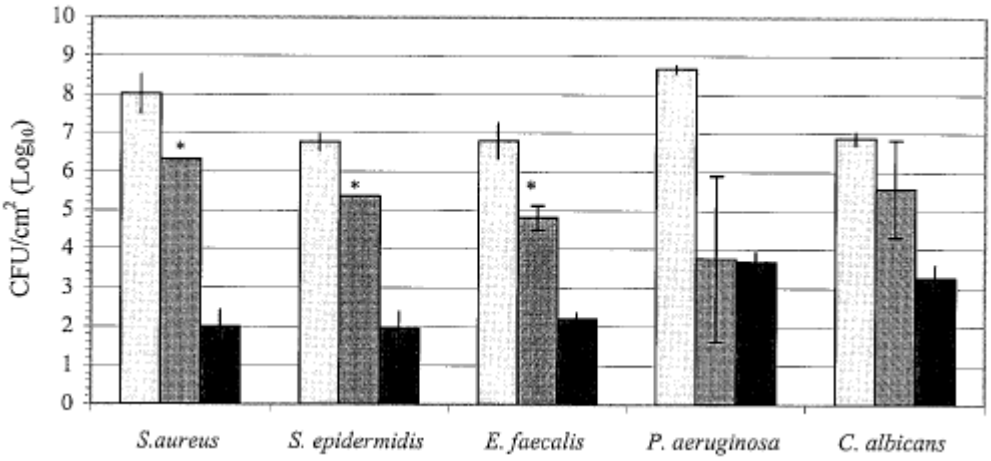

Figure 2.5 - Impact of Taurolidine and Citrate on Bacteria. Light shading represents initial live counts. Medium shading represents viable counts for heparin treated substrates. Dark shading represents viable counts for taurolidine-citrate coated substrates. Adapted from (Shah *et al.*, 2002)

The viability of *S. epidermidis* and *S. aureus* were reduced by several logs upon exposure to taurolidine and citrate coated substrates. This reaction is important since these bacteria are present in over half of all biofilms associated with CRBSI (Depuydt *et al.*, 2005).

Due to these promising results, the combined components are sold by Bio-Implant HandelsGmbH under the name Taurolock™. This product is mostly used for short-term applications such as intravenous catheters (TauroPharm GmbH, 2005).

2.4.5 - Furanones

There have been many previous studies that explored coating catheters with antibiotics such as vancomycin, teicoplanin, cefazolin, minocycline-rifampin and other types of coatings such as silver, chlorohexidine and salicylic acid (Hume *et al.*, 2004). Unfortunately none have proven to be both safe and serve as long-term protection against the formation of biofilms (Hume *et al.*, 2004).

Silver, for example, is toxic for mammalian cells. Other compounds containing silver such as chlorhexidine-silver sulfadiazine have also been associated with harmful side effects (Schmitt *et al.*, 1998). Bacteria have a resounding ability to adapt to antibiotics and it is unlikely any of the aforementioned could serve as long-term solutions (Hume *et al.*, 2004).

A novel approach for preventing comes from a group of chemicals called furanones. Furanones are a chemical defense found in the marine alga *Delisea pulchra* that prevent adhesion of other marine organisms. Researchers postulated that the furanones would also work against the *S. epidermidis* biofilm (Hume *et al.*, 2004).

For simplicity the researchers used the furanone 3-(1'-bromohexyl)-5-dibromomethylene-2(5 H). Results were compared with an azide layer, 4-azidoaniline, which served as the control, bare polystyrene as the process control, and the antibiotic combination of rifampin and minocycline (Hume *et al.*, 2004).

Both *in vivo* and *in vitro* studies yielded promising results. In all studies, furanone outperformed all other coatings. *S. epidermidis* did not grow well on such surfaces, as seen in Figure 2.6. *In vivo* studies conducted in sheep for 65 days demonstrated that furanones could be applied onto catheters and be effective against *S. epidermidis* throughout the duration.

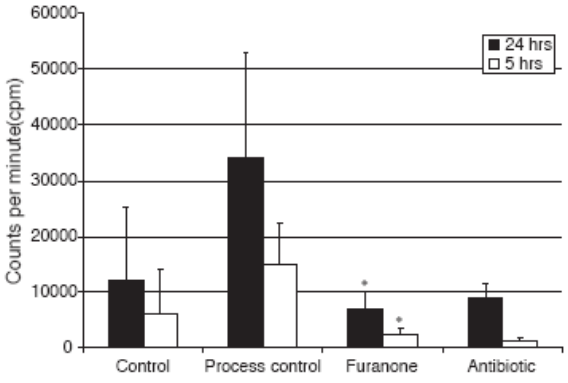

Figure 2.6 – *In vivo* Study Results of Furanone. Process Control group that were intentionally infected with *S. epidermidis* had highest rate of infection. Adapted from (Hume *et al.*, 2004)

Currently the mechanism behind furanones' anti-adhesive characteristics is not understood, but has potential for future applications. Although not commercially available, chances are favorable for such a coating to be applied in both short and long-term implanted catheters. The study lasted a total of two years and at the beginning, catheters were coated with furanones and were still active by the end of the study (Hume *et al.*, 2004). Potential applications could go beyond intravenous catheters and be extended to other medically implanted devices such as artificial hearts or hip replacements. Also, furanones are unlikely to induce bacterial resistance because unlike antibiotics, furanones only inhibit bacterial adherence and growth (Hume *et al.*, 2004).

2.5 SAMs

2.5.1 – SAM Characteristics

SAMs, or self assembled monolayers, were first introduced in 1946 by Zisman when he prepared a monomolecular layer on a metallic surface (Bigelow *et al.,* 1946). Since that time, alkanethiolates are the most studied SAMs. In terms of bacterial adhesion, some of the commonly studied behaviors of SAMs include wettability and

chemical reactivity. SAMs are exciting for use in surface engineering because they provide a uniform surface. Surface energies from SAMs can vary greatly. They can have properties similar to Teflon, which has a low energy, to highly energetic surfaces with -OH or -COOH groups (Ulman, 1996).

For microbiologists interested in preventing biofilm formation on catheters, SAMs are a logical area of study because of their easy preparation and uniformity. The versatility of the SAM is that by making changes at the molecular level, the substrate's overall characteristics will be completely altered (Ulman, 1996).

One of the problems with SAMs is ensuring their stability. Surface instability of SAMs comes in the form of surface reorganization. In fixed monolayers, a decrease in surface free energy occurs due to an increase of -OH groups (Ulman, 1996). Increasing surface free energy catalyzes substrate reorganization. The amount of reorganization of a SAM may be expressed as a function of a monolayer's melting point. Factors that may enhance the drive for substrate reorganization include temperature, relative humidity, and adsorption at the monolayer surface (Ulman, 1996).

2.5.2 Catheter Properties and SAMs

There is great interest in finding a material that can coat a catheter to prevent biofilms from forming. While much research has gone into this, commercially available polymers used in catheters can limit infection. For example, polypropylene (PP) has been found to limit bacterial infections, but polytetrafluoroethylene (e-PTFE) does not inhibit bacterial adhesion (Gottenbos *et al.*, 1999). One study's goal was to explore commonly used materials in catheters and determine how well *S. epidermidis* (HBH_2 102) and *Pseudomonas aeruginosa* (AK1) adhere and grow on the materials. The

materials studied included poly(dimethyl siloxane) (SR), polyethylene (PE), polypropylene (PP), polyurethane (PUR), poly(ethylene terephthalate) (PET), poly(methyl methacrylate) (PMMA), and glass (Gottenbos *et al.*, 1999).

Experiments were carried out in a flow chamber and the cells were perfused through the system for one hour. A video camera was mounted to focus on the material of interest and the liquid flow was not recirculated during the experiment (Gottenbos *et al.*, 1999). The initial experiments tried to create a correlation between hydrophobicity and initial cell adhesion. Water contact angles ranged from 20-111° and were compared to cell counts on all substrates. Unfortunately, there was not a significant difference between cellular retention on glass, which was the most hydrophilic, and SR, which was the most hydrophobic (Gottenbos *et al.*, 1999).

TSB was introduced into the flow chamber and biofilm development was analyzed (Gottenbos *et al.*, 1999)

$$n_i = n_0(2^{\Delta t/g} - k_{des}\Delta t)^i \qquad (26)$$

where n_i is the number of bacteria adhering after time Δt, n_o is the bacterial number at the start of the growth phase, g is the generation time, and k_{des} is the desorption rate constant (Gottenbos *et al.*, 1999).

Two separate experiments were carried out using full TSB and TSB that was 20 times diluted in water. After 24 hours in the flow cells with solution that was 20 times diluted, it was found that PP had the fewest bacteria, with only 6% of the substrate covered with *S. epidermidis*. This result was expected since clinically, PP is found to be resistant to biofilm formation. SR had the highest adherence with 80% of the surface

covered with bacteria. When the same experiment was carried out in 100% TSB, ~100% of all substrates were coated (Gottenbos *et al.*, 1999).

From these experiments it was concluded that initial adhesion is not proportional to bacterial growth. The water contact angle did not appear to correlate with the initial adhesion, although it may have related to the growth of bacteria. The more hydrophobic surfaces had the least bacterial growth (Gottenbos *et al.*, 1999).

2.5.3 – SAMs in Conjunction with Tri(ethylene glycol)

The use of SAMs to inhibit bacterial adhesion is largely in development. Since SAMs are simple to assemble, they easily alter substrate characteristics on a macroscopic scale (Ulman, 1996). A study experimented with a mixture of SAMs on a single gold substrate to explore how cellular adhesion was affected. *E. coli* strain RB 128, which is a clinical isolate, was used in these experiments (Qian *et al.*, 2002).

Eight unique experiments were carried out, incorporating varying SAM compositions. The chemicals composing the SAMs included Methyl α-D-mannopyranoside, *p*-amineophenyl α-D-mannopyranoside, *p*-amineophenyl β-D-galactopyranoside, 11-[(3-(α-D-Mannopyranosyl)propyl)thioethylaminecarbonyl Methoxy Hexa(ethoxy)undec-1-yl-thiol (MMH), tri(ethylene glycol), hex(ethylene glycol), and oligo(ethylene glycol) (Qian *et al.*, 2002).

These experiments showed that tri(ethylene oxide) resulted in complete inhibition of bacterial retention. This was an expected result from earlier studies that found 99.7% fewer bacteria on gold substrates coated with oligo(ethylene glycol) as opposed to bare gold substrates (Ista *et al.* 1996). Moreover, when tri(ethylene oxide) was mixed with other chemicals, the results were altered. In cases where the tri(ethylene oxide) was

mixed with MMH at varying concentrations ranging from 1% of the solution to 0.01% of the solution, bacteria readily adhered to the substrate. These results were expected since bacteria displaying multiple pilus attach to the mannoside ligands of the MMH SAM. The number of bacteria adhering to the substrate with varying concentrations of MMH resulted in no change, meaning that even a small amount of MMH promotes adhesion between bacteria and a substrate, despite tri(ethylene oxide) composing >99% of the SAM (Qian *et al.*, 2002).

Of the other SAMs, *p*-amineophenyl α-D-mannopyranoside was most promising, since the smallest area of the well lit up under fluorescence microscopy. This result is explainable since the chemical is known as a monomeric inhibitor for type 1 pili adhesion (Qian *et al.*, 2002).

2.5.4 – Study Incorporating Fibronectin (FN) with SAMs

FN is a protein found in the bloodstream that enables bonding between collagen, fibrin, heparin, and cells. Due to the importance of FN to allow cells and proteins to adhere to a site *in vivo*, it has been long theorized that bacterial adhesion is promoted when this protein adheres to a substrate. FN has a molecular weight of ≈ 450 kDa and is a large glycoprotein consisting of two polypeptide chains of nearly equal size (Plummer *et al.*, 2003).

The goal of studying FN in conjunction with SAMs was to see if SAMs can create gradients in the concentration of FN adhering to a substrate. If so, the researchers would continue to explore whether this gradient of FN alters the adhesion of 3T3 fibroblast cells (Plummer *et al.*, 2003).

The SAMs explored include 11-mercaptoundecanoic acid (MUA), 11-mercaptounddecanol (MUD), and 1-octanethiol (OT). Gold-layered glass slides were created, followed by adhering SAMs onto the substrate. MUD was usually first used to soak the substrate and then it was backfilled with MUA, which achieved the most consistent results (Plummer *et al.*, 2003).

The point of producing FN gradients was to observe how fibroblast cells were affected in terms of adhesion, spreading, and motility. The study aimed to produce a method that can be used to better understand immune response to infection, embryonic development, the closure of wounds, and the spread of cancer. Since FN is present on every single case of a CRBSI and is vital for cellular adhesion, this protein is very important to understand (Plummer *et al.*, 2003).

On a gold-covered glass slide, the gradient was between FN on one side and then a gradient transitioning to MUD on the other. The fibroblast cells adhered well and spread on FN, but on MUD, the cells did not adhere. The study demonstrated an ability to control cell adhesion and motility with FN gradients. More importantly, the way the gradients were made only requires solvent-accessible amines. Therefore, these findings are not limited to FN, but can be applied to other macromolecules for the study of cellular retention and motility (Plummer *et al.*, 2003).

2.5.5 - AFM study of SAMs

A novel approach to studying SAMs has been made possible through the invention of the Atomic Force Microscope (AFM). A study was done to analyze what effects the octadecyltrichlorosilane SAM had on neutrophil motility when in contact with one another. The AFM was important in obtaining time series topographical information

of the neutrophils on the SAM. Residual tail traces left by the cells were also detected by the AFM. The AFM software allowed the researchers to easily determine the distance the cells had moved in a given time frame (Zhou *et al.*, 2004). The researchers mainly used the AFM for photographing topography of the cells, but the AFM has many more functions that will be discussed in the following section.

2.6 – AFM

2.6.1 – General Overview

The AFM is a relatively new instrument that measures the forces between probe and substrate at the atomic level. In 1986, three inventors of the Scanning Tunneling Microscope (STM), Ernst Ruska, Gerd Binnig, and Heinrich Rohrer, shared the Nobel Prize for their achievement in Physics. The STM was later adapted into the AFM, which is much more versatile than the STM, in terms of the types of samples that can be examined. The AFM has presented a revolutionary new method to study an array of disciplines including microbiology (The Nobel Foundation, 1986).

The AFM operates by measuring both the attractive and repulsive forces between a microscopic tip and a sample. Several methods can be used to measure different forces including contact mode, non-contact mode, and tapping mode, as the most commonly used (Baselt, 1993).

Contact mode allows the user to move the tip onto a sample. Once on the surface, the tip may be dragged over the substrate. Two side-by-side photodiodes detect laser deflection off the cantilever that measures the vertical deflection of the tip, which is used to calculate the sample height. Contact mode can also be used to measure how ‘sticky’ a sample is by retracting the tip and measuring the forces as a function of distance.

Contact mode is fast to use and best for hard surfaces such that the tip does not damage the sample (Baselt, 1993).

When used in air or other gases, tapping mode is commonly used at frequencies of several hundred kHz. It can be used in liquid, but the frequencies would be different. Tapping mode is in essence contact mode but the interaction between probe and substrate is for very brief time intervals. When attempting to image topographical information of a sample that is soft or could be damaged by the probe, tapping mode would be the best choice. It is suspected that the resulting image of using this function is directly related to both the stiffness and elasticity of the sample. Tapping mode is slower than contact mode and is best for softer samples that would otherwise be damaged (Baselt, 1993).

In non-contact mode, the tip and sample are maintained at a small distance from one another, such that the attractive forces between tip and sample can be measured. Less commonly used, the user must be careful to avoid the tip moving too close to the surface and keep the tip close enough such that forces can be detected (Baselt, 1993).

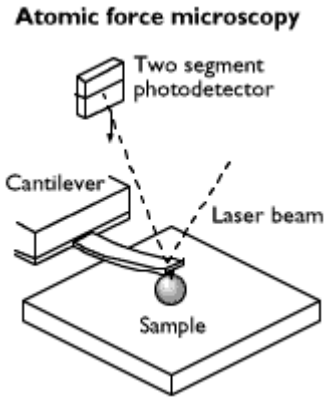

Figure 2.7 – Representation of AFM Measuring Topographical Data, adapted from (Baselt, 2006)

2.6.2 - Tips

The operator of the AFM has the choice of many cantilevers made of several different substances. Since most operations are carried out in air using contact mode or tapping mode, the tips most often used would be the ones designed for such an operation. The cantilevers are often made of silicon and coated by various substances. The most widely used coatings include titanium-platinum, chromium-gold, copper-chromium, and Si_3N_4 (MikroMasch, 2006). The purpose of the coatings is to increase laser beam reflection and prevent the cantilever from bending. The choices available vary in terms of hydrophobicity, reflectance, and magnetism. The coating that the researcher uses depends on the requirements of a particular experiment. For example, the copper-chromium tip is magnetic and would be ideal for exploring the magnetic properties of bacteria (MikroMasch, 2006). The manufacturer also offers an option to have the backside of the cantilever coated with either aluminum or gold-chromium. In both cases, the advantage would be to increase reflectance from the laser. No coating adds stress onto the cantilever, which can lead to bending (MikroMasch, 2006).

Each tip is carefully manufactured so that it has a specific spring constant, length, width, height, and resonance frequency. Each tip has a unique spring constant, which also yields a different resonance frequency (Baselt, 2006)

$$frequency = \frac{1}{2\pi}\sqrt{\frac{spring\,\text{constant}}{\text{mass}}} \tag{27}$$

The geometric shape of the tip is important. Had the manufacturer used a slinky, the time required to respond to the features of a sample would be increased. A slinky has a spring constant of ~1 N/m and passing the spring over a sample would require a greater

downward motion. A flexible stylus has a spring constant of ~0.1 N/m, meaning it is less likely to damage a sample (Baselt, 2006).

The cantilever can be a variety of lengths, usually between 100-200 μm. The cantilever tip usually comes in three varieties; a 'normal' pyramidal shaped tip, a supertip that has a rod extending from the tip of the pyramid, and an ultralever that is in the shape of a sharp rod extending up directly from the cantilever. Tips are usually ~3 μm in height (Baselt, 2006).

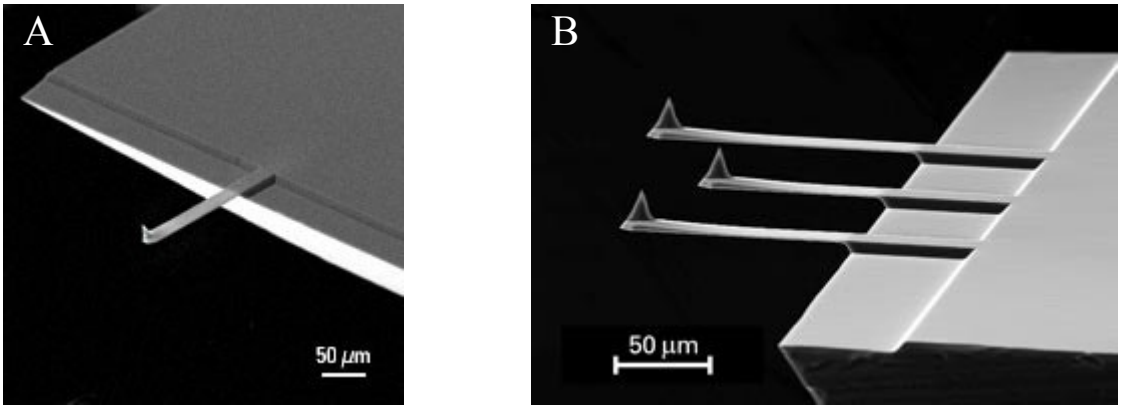

Figure 2.8 – (a) SEM image of silicon tip coated with Ti-Pt (b) SEM image of 3 silicon tips coated with Aluminum. Adapted from (MikroMasch, 2006)

2.6.3 - AFM Analysis

The topographical information may be analyzed with a variety of methods such as the section analysis and roughness analysis. These tools allow the user to quantify information from an image taken of a substrate (Baselt, 2006). If, for example, the substrate is identified, then the dimensions of the deposits on the substrate can be measured. These tools can be used to yield statistical data that, in the case of bacteria, may be used to explain characteristics of adhesion, viability, or changes in morphology (Simon and Durrieu, 2006).

2.6.4 - Cantilever Calibration

Researchers that use the AFM need simple methods to determine the exact characteristics of the cantilevers being used. According to Burnham *et al.*, there are four methods of determining the cantilever stiffness. Two of the methods utilize 'geometric' parameters since the dimensions of the beam are found in the stiffness equation (Burnham *et al.*, 2003). The other two are known as 'thermal' methods because they are based on square of the fluctuations in amplitude as a function of frequency (Burnham *et al.*, 2003).

2.6.5 - AFM Applications

Recent AFM applications have been to study cells since it is minimally invasive using a standard tip. Imaging of cells is limited to topographical information and in eukaryotes, structures such as nuclei, mitochondria, and cytoskeletal filaments have been observed. Current methods of AFM are too slow to study many biochemical or biological processes in real time, due to the scanning rate of the machines. Improvements in the AFM will be to increase resolution and scan rate. Currently, the AFM is most useful in obtaining force curves that yield mechanical properties of cells (Simon and Durrieu, 2006).

Cellular mechanical, or nanomechanical, properties can be determined through force measurements made with the AFM. One method of producing a force curve is by examining height images at a constant load. The topographical and mechanical image of indenting a cell with a tip at multiple locations yields a height profile. This height profile deduces the elastic modulus, G, from where F, the force, may be measured (Simon and Durrieu, 2006)

$$F=k\delta=\Pi G\Phi l(1-\nu^2) \quad (28)$$

where δ is the cantilever deflection, k is the local stiffness, G is the elastic modulus, and Φ is the diameter of the contact area (Simon and Durrieu, 2006).

The elastic properties of different cells have been probed with the AFM. Cardiac cells, for example, are some of the stiffest at 100 kPa, while endothelial cells are soft at 1.4-1.7 kPa. No two cells have the same mechanical properties, which depends on their function. Elasticity also varies depending on the location of the cell that the tip is interacting with (Simon and Durrieu, 2006).

Studying cellular adhesion forces to substrates is one of the important functions of the AFM. AFM may reveal changes in morphology by cellular adhesion due to the presence of stress fibers. In addition, the cell's stability may be measured when undergoing a load or being effected by drugs (Simon and Durrieu, 2006).

Another method of studying cellular adhesion to surfaces is by measuring the displacement force required to remove the cell. This is accomplished by measuring a laser deflection to lateral cantilever displacement. The method can be used to calculate the speed cellular adhesion takes place, the distance required to remove the cantilever until the adhesion force is null, and the overall force with which a cell adheres to a surface. Adhesion forces can be measured versus time, temperature, and hydrophobicity of a surface (Simon and Durrieu, 2006).

AFM is not limited to measuring cell to substrate adhesion forces, but can also measure cell to cell adhesion forces. Such experiments ideally consist of three stages:

1. Contacting the tip coated with a single bacterium to a monolayer at a known force.

2. Leaving in contact for a desired time.
3. Retracting the tip and breaking any bond between bacterium and monolayer.

In the first step, repulsive forces can be measured between cells. After sufficient time, the force required to separate cells can also be measured. The procedure must be repeated many times with varying contact times between cells to ensure reproducible results (Simon and Durrieu, 2006).

Forces between human uterine epithelial cells (HEC-1-A, RL95-2) and human trophoblast-type cells (JAR) were measured with AFM. Initially there were repulsive forces between cells as they approached one another and with HEC-1-A displaying higher values of repulsion than RL95-2. The authors had previously shown that RL95-2 cells have a thinner glycocalyx layer than HEC-1-A. The force between JAR and HEC decreased in increments of <200 pN following separation. RL and HEC on the other hand displayed rupture events with increments of 1-3 nN. Such a large separation force may be attributed to strong cell-to-cell bonds (Simon and Durrieu, 2006).

2.6.6 - AFM Study of *S. epidermidis* Biofilms

The many applications of the AFM have enabled researchers to explore the effects antimicrobials have against biofilms. Silver ions bind to thio, amino, carboxylate, imidazole, and phosphate groups of molecules, and inhibit bacterial viability by disrupting metabolic activity. In addition, silver ions displace metals necessary to bacterial survival such as Ca^{2+} and Zn^{2+}. Chaw *et al.* conducted a study with *S, epidermidis* biofilms by introducing them to silver ions to induce cellular mortality and disrupt the overall biofilm structure.

Two strains of *S. epidermidis* were used in the experiment; RP62A, notable for accumulation-associated proteins, and strain 1457 that produces the polysaccharide intercellular adhesion (PIA). The study explored the effects of silver ions on the bacteria through plate counting, SEM, and AFM. Silver ions at a concentration of 50 ppb were added to the wells following cell growth of 4, 7, and 12 days. Cells were exposed to silver ions for 5, 10, 30, and 60 minutes (Chaw *et al.*, 2005).

Based on plate counts, there was little difference between the control group and bacteria exposed to the silver ions in terms of viability (Chaw *et al.*, 2005). Moreover, SEM images revealed more information on how silver ions affected the biofilms. In all instances, the silver ions had penetrated the biofilms; thus disrupting the once organized structures. The disrupted zones of the biofilms were 10-25 μm in width after 4 days, 30-40 μm after 7 days and 60-100 μm after 12 μm (Chaw *et al.*, 2005).

In the AFM portion of the study, the force curves during which the cantilever tip coated with polyethylencimine approached the biofilm were identical. As the tip approached the EPS, it was repelled by electrostatic double-layer interactions. Following this, the tip then encountered a strong attractive at close range force due to a negative net force toward the substrate. The force curves also demonstrated the compliant nature of the soft cellular surfaces (Chaw *et al.*, 2005).

Retraction curves revealed differences between the control group and the group exposed to silver ions. The forces measured in the group exposed to silver ions were between 0.1 and 4.0 nN, with forces extending up to 5-15 nm. For the control group, the breakage point was found to be about 16 nN at a displacement of 30 nm. The disruption of the EPS is likely due to silver ions binding to proteins and polysaccharides composing

the EPS. Although the use of silver ions is promising in regards to disrupting biofilms, it mostly failed to affect cell viability. Used in conjunction with antibiotics, silver ions may prove more effective since antibiotics have difficulty penetrating the EPS (Chaw *et al.*, 2005).

3.0 Materials and Methods

3.1 – Cell Culturing

A clinical isolate of *S. epidermidis* was kindly provided by Dr. Stephen Heard from the University of Massachusetts Medical Center (Worcester, MA). Cells were maintained at 4°C on Tryptic Soy Agar (TSA) (Sigma, USA) plates. To culture the bacteria, colonies were streaked from the TSA plate and placed in a culture flask with 10 mL of TSB (30 g/L) (Sigma, USA). The cells were pre-cultured overnight (~14 hours) in an incubator at 37°C. A 0.5 mL sample of precultured cells was transferred to a 250 mL Erlenmeyer flask containing 50 mL fresh TSB. All culturing took place in a level II hood (The Baker Company, Inc., USA) with the air blower on, to avoid contamination. The flask was sealed with aluminum foil across the top and was placed into a water shaker bath at 37°C for approximately 2-3 hours until the cells reached the mid-exponential phase, as determined by measuring the absorbance at 600 nm with a spectrophotometer (Thermo Spectronic, USA). Initially, the absorbance was measured every 15-30 minutes so that a bacterial growth curve could be created. These readings were compared to cellular densities verified using a counting chamber.

The counting chamber was flooded with ethanol to remove residue, and a nitrogen blower was used to quickly dry the counting chamber. Prior to cells being injected into the device, the microscope, with a 60x objective, was used to scan the surface and verify cleanliness. Cells suspended in MES buffer solution were then injected into the counting chamber and pictures were taken of 15 randomly chosen grids for each of six absorbance readings (Figure 3.1). Each grid has a volume of 0.1 μl.

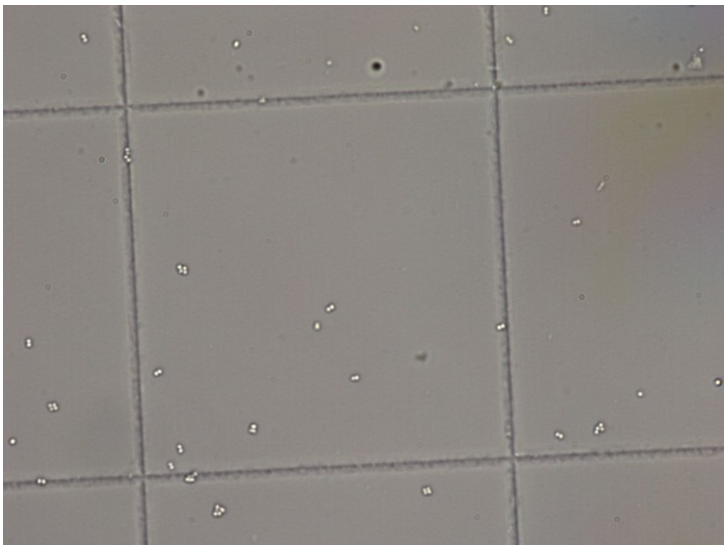

Figure 3.1 – *S. epidermidis* in a Counting Chamber (600X Magnification)

The doubling time for the bacteria in the exponential phase was calculated using the following

$$N = N_0 \times 2^{kt} \tag{29}$$

where N_0 is the initial population, k is the growth constant, and t is the time. This calculation was used to ensure that bacteria are always harvested during the mid-exponential phase.

Cells were washed and removed from TSB solution by centrifugation at 190 g for 15 minutes. The supernatant was removed and replaced by autoclaved 0.1 M MES buffer at pH=6.1 (2-(N-Morpholino)ethanesulfonic acid). Following resuspension, bacteria were diluted in 0.1 M MES, to a final of concentration of 2.0×10^7 cells/mL.

3.2 – Autoclaving

All lab equipment used during the experiments was sterilized. It is especially important that no other bacteria are present during inoculation of the growth media.

Some of the single use equipment such as Petri dishes and centrifuge tubes arrived sterile. The pipette tips were individually placed in a small bin that is autoclaveable. Autoclave indicator tape was wrapped around the edges. The inoculation rings were autoclaved in an autoclave-safe metal container and autoclave tape was wrapped on the container.

Growth media and buffer solutions were prepared in the manufacturer recommended concentrations. Solutes were weighed on an electronic scale (OHAUS Corporation, Switzerland) and then funneled into 1-liter Erlenmeyer flasks. Once the necessary quantity of liquid and solute was added, an oval magnet was dropped into the flask and a magnetic stirrer (VWR, USA) was used until the solute was completely dissolved. The magnet was removed and the top of the flask was sealed with two layers of aluminum foil, and firmly taped to ensure liquid would not evaporate during the autoclave process. For each 200 mL of prepared solution, the autoclave was run for 15 minutes (121° C and 30 PSIG).

3.3 – Preparation of SAMs

We examined the retention and viability of *S. epidermidis* on various substrates including glass, gold, and SAMs with terminal groups that contained isopthalic acid (IPA), isopthalic acid with silver (IAG), tri-ethylene glycol (TEG), and pyridine decanethiol (PYR).

The slides (Evaporated Metal Films, USA) had dimensions of 75 mm x 25 mm x 1 mm and were coated with 5 nm chromium followed by 100 nm of gold. The gold portion was made of 9 ppm silver. Surface debris was removed by immersing the gold slide in piranha solution (70% sulfuric acid and 30% hydrogen peroxide) for 10 minutes at 90 °C. Slides were thoroughly rinsed with distilled water, 100% ethanol, and dried in a

nitrogen stream. Slides should be used immediately following cleaning, but storage in 100% ethanol for several days is also possible.

3.4 - Preparation of Glass Slides

The glass slides, measuring 25x75x1 mm (Erie Scientific Company, USA), were prepared in 3:1 HCl/HNO_3 for 25 minutes, rinsed in distilled water, and immersed in 4:1 H_2SO_4/H_2O_2 for another 25 minutes.

The chemically-modified surfaces were prepared by Ernesto Ruben Soto Villatoro and Eftim Milkani. TEG was prepared using procedures found in literature (Pale-Grosdemange *et al.*, 1991), as was IPA (Soto *et al.*, 2003) and PYR (Hu and Fox, 1999). IAG was prepared by immersing an IPA slide in a 5 mM solution of silver (I) nitrate in acetonitrile for 3 hours. The presences and properties of the SAMs were verified using a variety of methods including AFM, NMR (nuclear magnetic resonance), CD, and contact angles.

3.5 – Batch Experiments for Quantifying Bacterial Retention

The slide of interest was placed in a small Petri dish. Undiluted cells from the stock solution suspended in MES were pippeted directly on the slide. Then 4 mL of MES was placed on the slide to remove bacteria that were not well attached. The volume of cells from the stock solution was dropped on the slide such that the final concentration was 2.0×10^7 cells/mL. The Petri dish was placed in the incubator at 37°C for 30 minutes. Time variations of 1 hour and 24 hours were experimented with at concentrations of 2.0×10^9 cells/mL and 2.0×10^7 cells/mL. Following the incubation period, the liquid was pipetted out and solution was replaced with 4 mL MES buffer solution.

A *Bac*Light live/dead kit (Molecular Probes, USA) was employed to stain the cells. The kit was composed of two nucleic acid staining chemicals; 20 mM propidium iodide and 3.34 mM Syto 9. All cells were stained with Syto 9 and appear green under a FITC filter. Cells with compromised membranes were stained by propidium iodide and appear red under the Texas red filter. Cells stained by both dyes appear a lighter green under the FITC filter (Boulus *et al.*, 1999). The manufacturer suggests 3 μL of each dye per mL of bacterial suspension yielding a solution of 10 μM Syto 9 and 60 μM propidium iodide. However, this concentration was too high for Gram-positive bacteria and approximately a 100 fold dilution was determined to be sufficient, after a trial-and-error process to determine the optimal dye concentrations.

Both Syto 9 and propidium iodide are light sensitive; therefore all operations with these chemicals were conducted with minimal lighting. Syto 9 was first diluted 10 fold in DMSO (Sigma, USA) solution. Then 10 μL was added to the 4 mL of the bacterial solution such that the concentration was 0.835 μM Syto 9. Propidium iodide was initially diluted 100 fold in DMSO and then 10 μL was added to the 4 mL bacteria solution such that the concentration was 0.5 μM. After 10 minutes, the cells were ready for viewing.

Digital photographs were taken using a Nikon Eclipse E400 (Nikon, Japan) with a mounted 18.2 Color Mosaic Camera (Diagnostic Instruments, Inc, USA). The fluorescence light was powered by a Mercury-100 W lamp (Chiu Technical Corporation, USA). The image was magnified by a 100x objective lens and light was passed through Texas Red and FITC filters (Nikon, Japan). The total area was measured using the Spot Advanced software (Diagnostic Instruments, Inc., USA) to quantify the total

concentration of bacteria. Fifteen locations were randomly chosen per slide and in each case, the entire photo was analyzed.

The Spot Advanced software can take individual pictures of cells stained by propidium iodide and Syto 9. The software allows for pictures to be overlapped to make counting easier.

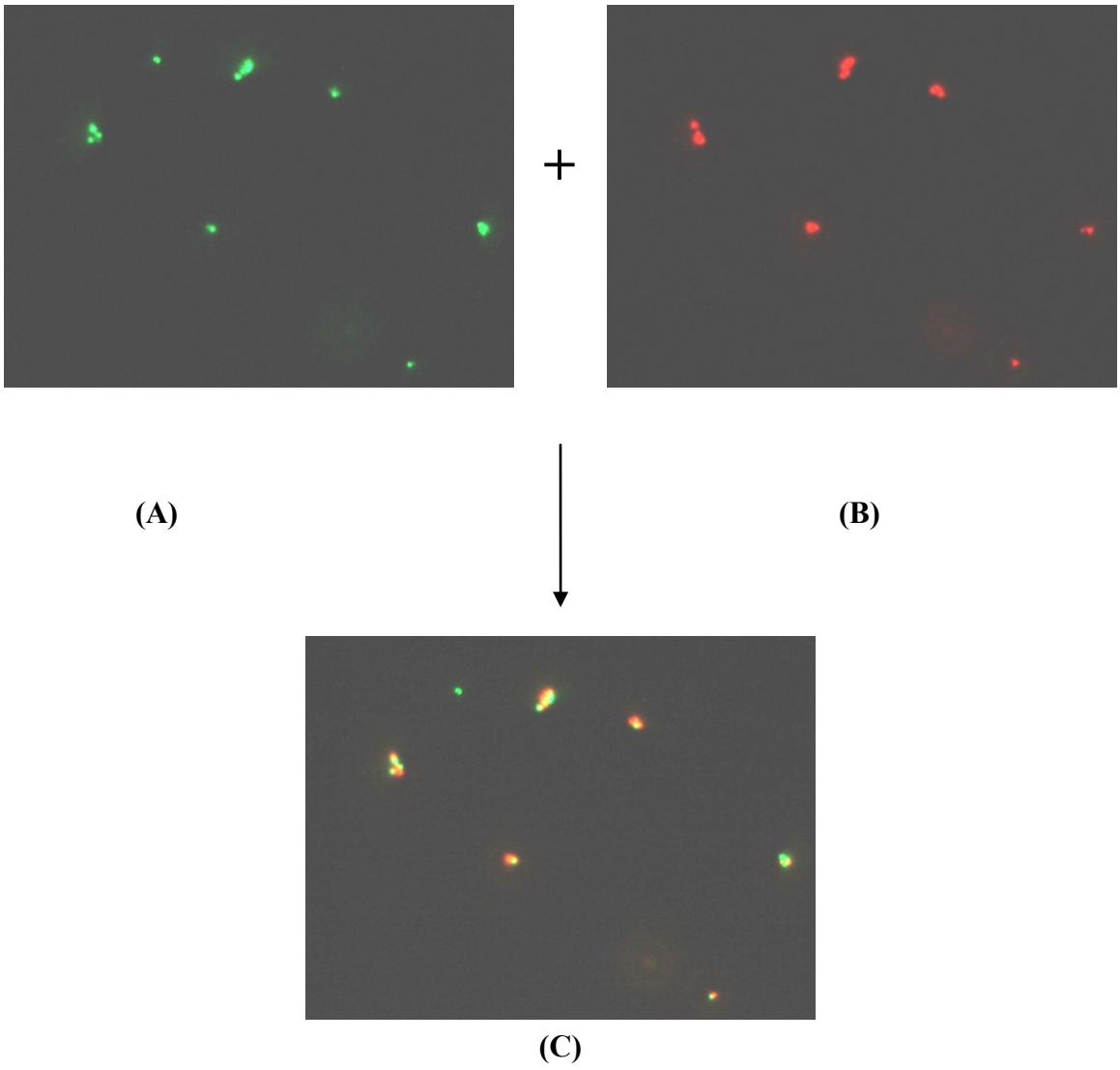

Figure 3.2 – Fluorescence Microscopy of *S. epidermidis* on Gold Substrate. Area of 0.158 mm^2**.** Viewed by a (A) FITC filter, (B) Texas Red filter, and (C) Digitally Combined Photo (Photos enhanced by Photoshop to improve contrast)

3.6 – Protein Deposistion and Bacterial Retention in the Presence of Protein

Fetal bovine serum (FBS) (Atlanta Biologicals, USA) was applied to the aforementioned substrates to measure changes in cell viability or adhesion in the presence of protein. FBS was stored frozen at -5 to -10°C and thawed before use. Cleaned slides were immersed in 4 mL 10% FBS/ 90% MES buffer solution for 80 minutes at 37°C. Other concentrations of FBS were considered for these experiments including 10%, 50%, and 100%. The solution was pippeted out and replaced with 100% MES solution. The procedure then continued by soaking the slide in 0.1 M MES buffer with 2.0×10^7 cells/mL for 30 minutes, staining, and counting via fluorescence microscopy.

3.7 – Surface Free Energy and Contact Angles

SAM formation and cleanliness of the substrate was verified by measuring contact angles on the surfaces and calculating the free energies of the substrates, which included uncleaned gold, cleaned gold, IPA, IAG, gold + FBS, IPA + FBS, and IAG + FBS. Contact angles were measured with water, diiodomethane, and formamide at room temperature.

A camera was mounted such that it captured a droplet on the substrate of interest through a 20x objective lens. Many images were collected to ensure accuracy so that any possible out-of-focus images could be discarded.

The process of measuring the contact angle on the substrate worked best when two researchers were available. One person measured 2 μL droplets in a pipette and dropped them onto the substrate. It was important to use less than 5 μL liquid per drop so that effects of gravity may be ignored. The second person focused the picture/video and directed the first person as to when and where to release the droplet. The videos were

usually between 2 and 4 seconds in length but the only part analyzed was the instant the droplet was on the substrate and the pipette was retracted. When the liquid encountered spreading, only the video was analyzed. The photo required time for focusing and the shot was taken after spreading has occurred, which yielded inaccurate results.

Once all the pictures and videos were taken, first, the images needed analyzing to calculate the contact angle. A key assumption was that the droplet formed a section of a sphere. Printed out, a protractor and pencil (sharpened or 0.5 mm recommended) were the necessary materials to make the measurements for calculating the contact angles. The method to measuring contact angles was as follows:

1. A line was drawn through the middle of the droplet below the substrate.

2. From an edge of the droplet, an arbitrary line was drawn such that it went through the droplet to the edge.

3. A line was drawn perpendicular to the line just drawn until it crossed the centerline. This intersection was the midpoint of the pseudo-sphere.

4. From the intersection, a line was drawn to the respective edge of the droplet. This line was the radius of the pseudo-sphere. The distance from the center of the pseudo-sphere to the middle of the baseline of the droplet was labeled Y and the distance from midpoint of the droplet at the baseline to the edge of the droplet along the baseline was labeled X.

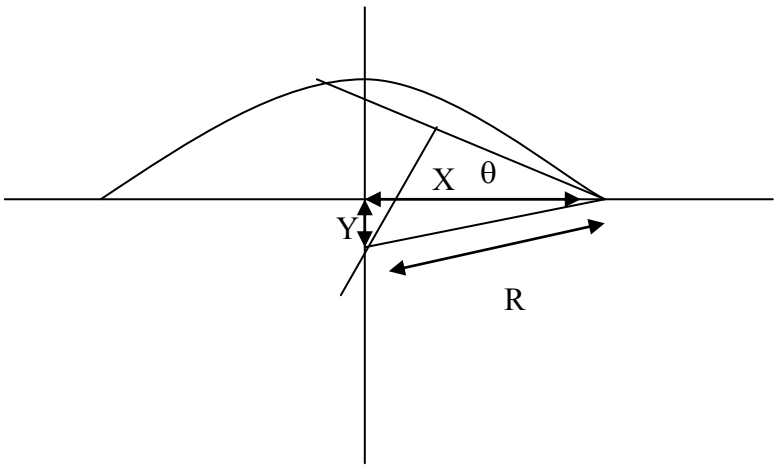

Figure 3.3 – Representation of Measuring Contact Angles

5. For each droplet, two contact angles were derived. Theoretically, the two angles from the same droplet were the same but may not be so due to experimental error or non-uniformity of the substrate. For each side, the angle, θ, was derived by using either

$$arcSin(\frac{X}{R}) = \theta \tag{30}$$

or

$$arcCos(\frac{Y}{R}) = \theta \tag{31}$$

The two derived values were averaged together to yield a contact angle for one side of the droplet.

6. In all cases, X, Y, and R made right triangles such that both cases should always be true:

$$X^2 + Y^2 - R^2 = 0 \tag{32}$$

and

$$\frac{X^2 + Y^2}{R^2} = 1 \tag{33}$$

The amount of error in equation 32 is unit dependent. If measurements, for example, were recorded in meters, then in all cases the final value would always likely be near 0, since the pictures were no larger than a few centimeters. On the other hand, if the measurements were taken in millimeters, then it is more likely that the resulting error would have been far from 0. Equation 33 is not unit dependent. Regardless if units were measured in kilometers or millimeters, the error would always be the same.

7. These data were best organized in a spreadsheet. For each contact angle correlating liquid to substrate, the data was averaged and the standard deviation found. Mathcad® or some other computer program may be employed to solve for the surface free energy.

8. Equations 34, 35, and 36 were solved in which case anything with a subscript *B* was an unknown parameter. Therefore, γ_B^{LW}, γ_B^+, and γ_B^- were all unknowns and were solved for. It is for that reason three separate liquids were used.

$$\gamma_W(\cos\theta_W + 1) = 2\cdot\sqrt{\gamma_B^{LW}\cdot\gamma_W^{LW}} + 2\cdot\sqrt{\gamma_B^+\cdot\gamma_W^-} + 2\cdot\sqrt{\gamma_B^-\cdot\gamma_W^+} \tag{34}$$

$$\gamma_D(\cos\theta_D + 1) = 2\cdot\sqrt{\gamma_B^{LW}\cdot\gamma_D^{LW}} + 2\cdot\sqrt{\gamma_B^+\cdot\gamma_D^-} + 2\cdot\sqrt{\gamma_B^-\cdot\gamma_D^+} \tag{35}$$

$$\gamma_F(\cos\theta_F + 1) = 2\cdot\sqrt{\gamma_B^{LW}\cdot\gamma_F^{LW}} + 2\cdot\sqrt{\gamma_B^+\cdot\gamma_F^-} + 2\cdot\sqrt{\gamma_B^-\cdot\gamma_F^+} \tag{36}$$

Solving equations 34, 35, and 36 simultaneously

$$\begin{bmatrix}\gamma_B^{LW}\\ \gamma_B^+\\ \gamma_B^-\end{bmatrix} = \left\{\left[2\cdot\begin{pmatrix}\sqrt{\gamma_W^{LW}} & \sqrt{\gamma_W^-} & \sqrt{\gamma_W^+}\\ \sqrt{\gamma_D^{LW}} & \sqrt{\gamma_D^-} & \sqrt{\gamma_D^+}\\ \sqrt{\gamma_F^{LW}} & \sqrt{\gamma_F^-} & \sqrt{\gamma_F^+}\end{pmatrix}\right]^{-1}\cdot\begin{pmatrix}\gamma_W\cdot[\cos(\theta_W)+1]\\ \gamma_D\cdot[\cos(\theta_D)+1]\\ \gamma_F\cdot[\cos(\theta_F)+1]\end{pmatrix}\right\}^2 \tag{37}$$

9. The acid-base electrical free interaction free energy (ΔG^{AB}) was calculated using the following

$$(\Delta G^{AB}) = 2 \times (\gamma^{-} \times \gamma^{+})^{0.5} \quad (38)$$

10. The surface tension (γ^{Total}) was then calculated using the following equation

$$\gamma^{Total} = \gamma^{AB} + \gamma^{LW} \quad (39)$$

where γ^{LW} is the Lifshitz-van der Waals tension and γ^{AB} is the acid-base surface tension.

3.8 – AFM Section Analysis

The section analysis operation within the AFM software (Nanoscope version 5.12r5) was used to acquire the vertical height information of each sample. The root-mean-squared roughness (R_{rms}, Eq. 40) was obtained with the same software, from measured areas of sizes ranging from (50×50) nm^2 to (200×200) nm^2, taking into account the features of interest of the samples.

$$R_{rms} = \sqrt{\frac{x_1^2 + x_2^2 + ... + x_N^2}{N}} \quad (40)$$

The AFM was used to characterize the gold substrates with different substrates in the presence of several buffers including 0.01 M sterile PBS, 0.1 M sterile MES, and 0.85% NaCl solution. The buffers were characterized on bare gold, gold soaked in 10% FBS for 80 minutes, and in 100% FBS for 80 minutes. The objective of these experiments was to determine which, if any, buffer was ideal for experimentation. It was preferable for the substrate to exhibit a low degree of deviation in terms of roughness to ensure uniformity. The AFM was operated in air; therefore the slides were dried before analysis. For each slide, when crystal formation was found on the substrate, data was taken from the crystal structure and underlying substrate separately.

4.0 – Results + Discussion

4.1 – Growth Curve

The microbial growth curve of *S. epidermidis* was created by measuring the absorbance readings as a function of time. The growth curve illustrates the stages of bacterial growth in TSB including the lag phase, log phase, and stationary phase (death phase not shown). More importantly, this plot shows when the bacteria enter the mid-exponential phase; a period when the cells are healthiest.

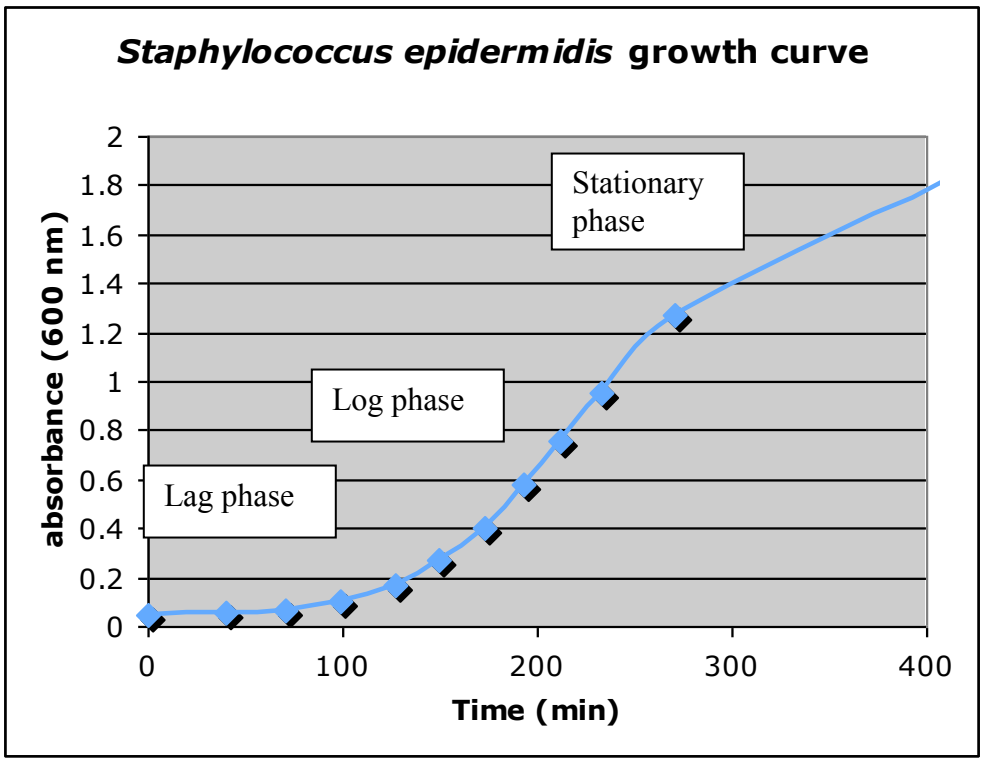

Figure 4.1 – Growth Curve of *S. epidermidis*

4.2 – Counting Chamber

Bacterial growth followed the expected pattern (Figures 4.1 & 4.2). A linear trendline very closely matched the data points.

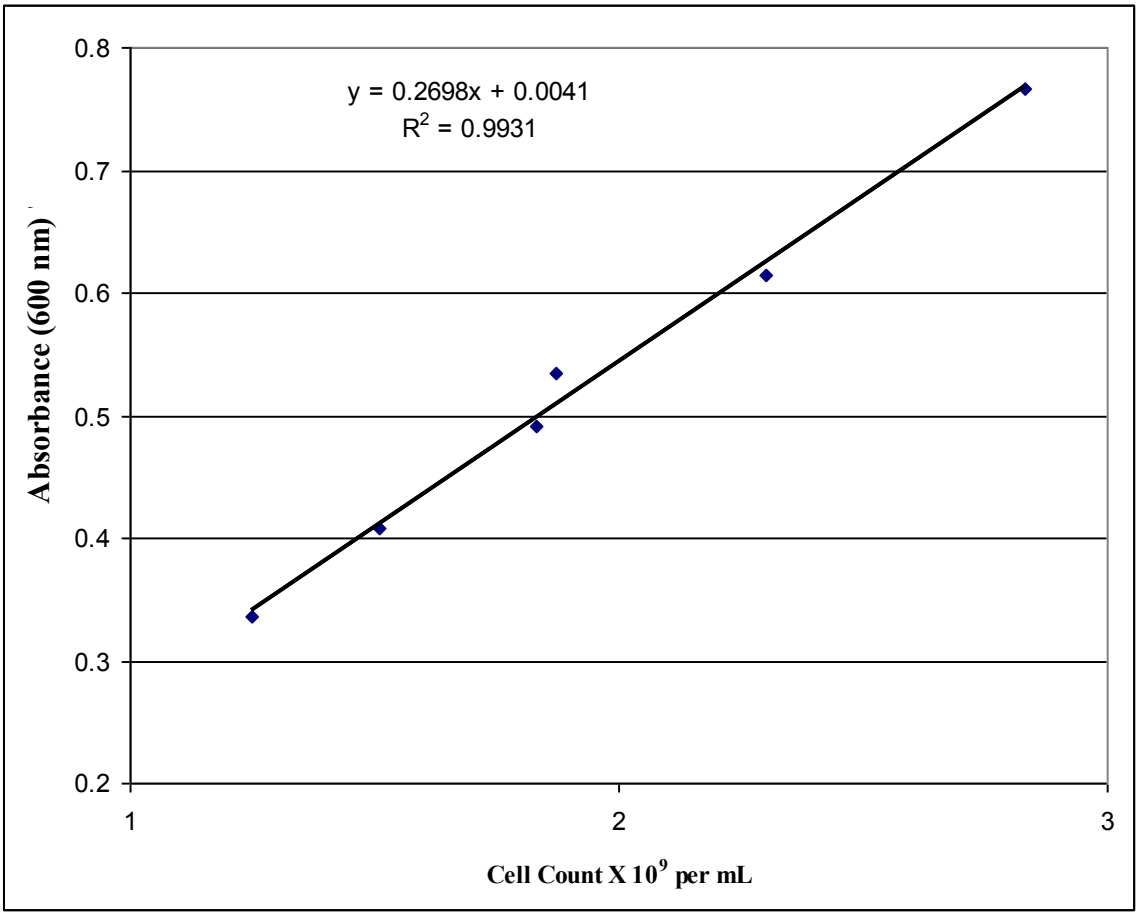

Figure 4.2 - Absorbance Readings vs. Cell Count

For each experiment, the goal was to have slides soaked in 2×10^{7} cells/mLand the above graph was used to calculate the dilution needed to achieve that concentration using

$$y = .2698x + 0.0041 \qquad (41)$$

where y is the absorbance reading from the spectrometer and x is the cell concentration 10^{-9} cells/mL. The mid-exponential phase was reached in ~2.5 hours and the cells could have been removed anytime from an absorbance of 0.3 to 0.8, but for consistency, the goal was to reach an absorbance of 0.5. After the cells were cultured, they remained in buffer solution for several hours at room temperature until the experiment was ready to

proceed. No difference in terms of viability of adhesion was found between cells used immediately following resuspension and cells used several hours later.

4.3 – Surface Tension and Contact Angles

Surface free energy was calculated by measuring contact angles between substrates and liquid water, diiodomethane, and formamide. The experiments were conducted between these liquids and uncleaned gold, acid cleaned gold, IPA, IAG, gold + FBS, IPA + FBS, and IAG + FBS.

For substrates without adhered proteins, the surface free energies were almost identical; ranging from 42.72-45.72 mJ/m^2 (Table 4.1). The same substrates were also hydrophobic. Contact angles between substrates and water ranged from about 70° to 90° (Table 4.1). These results were indicative of a favorable environment for bacterial adhesion.

Table 4.1 – Contact Angles and Surface Tension Calculations (mJ/m^2) for Substrates w/o Proteins

	water θ	Diiodomethane θ	Formamide θ	γ^{LW}	γ^{-}	γ^{+}	γ^{AB}	γ^{Total}
Unclean gold	89.18	28.58	63.45	42.327	2.023	0.019	0.390	42.72
Clean gold	70.67	16.09	59.09	42.183	16.095	0.194	3.573	45.72
IPA	71.75	27.23	51.23	40.215	9.930	0.187	2.730	42.94
IAG	75.40	28.39	51.81	40.580	6.880	0.246	2.600	43.18

Once the FBS was introduced to the substrate, there was a dramatic reduction in both the water contact angle and surface free energy. For the gold + FBS substrate, the water contact angle was 52°, which had experiments resulting in only moderate adhesion. For IAG and IPA + FBS, the surface free energy and contact angles were even further reduced. Surface free energies were 11.023 mJ/m^2 for IAG + FBS and 8.42 mJ/m^2 for IPA + FBS (Table 4.2). The same substrates were extremely hydrophilic. Water contact angles were 28.97° and 23.27°, respectively.

Table 4.2 – Contact Angles and Surface Tension Calculations (mJ/m^2) with FBS

	water θ	Diiodomethane θ	Formamide θ	γ^{LW}	γ^-	γ^+	γ^{AB}	γ^{Total}
IAG + FBS	28.97	81.97	81.97	7.53	123.09	0.025	3.5	11.023
IPA + FBS	23.27	82.07	79.28	7.41	126.03	2.03E-03	1.01	8.42
Gold + FBS	51.00	43.00	73.00	26.98	64.21	1.28	18.15	45.12

An interesting result from the experiments was that the combinations of two hydrophobic substrates yielded a surface that was hydrophilic. This is further evidence that the SAMs have an impact on bacterial adhesion despite the adherence of proteins. Figure 4.3 illustrates a relationship between the numbers of cells on the substrates to the surface free energy. Figure 4.4 compares the percent of dead cells per substrate versus the surface free energy.

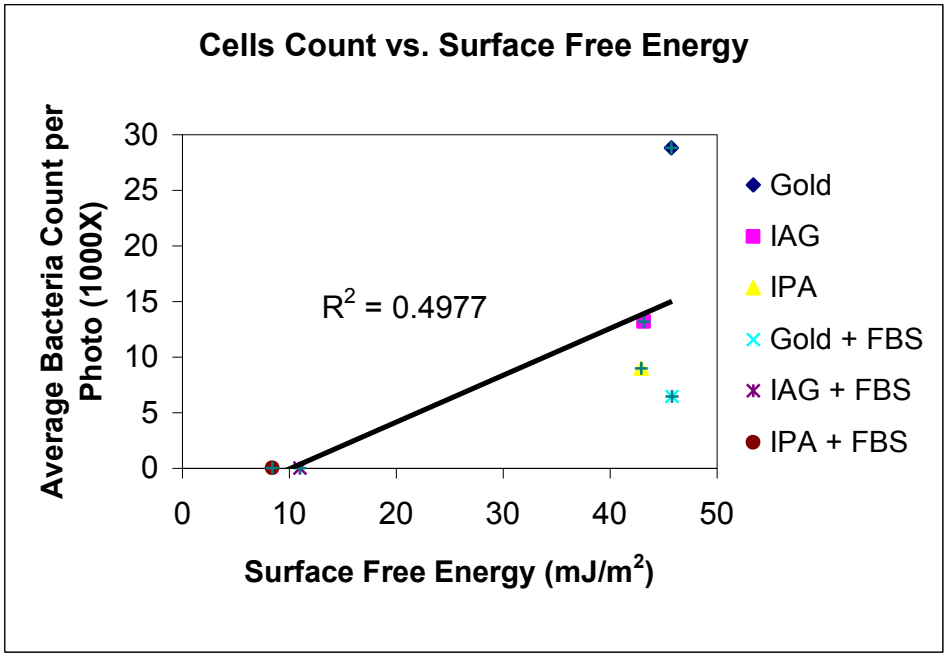

Figure 4.3 – Average Cell Count on Substrates per Photo vs. Surface Free Energy. Low surface free energy indicates reduced chance of adhesion.

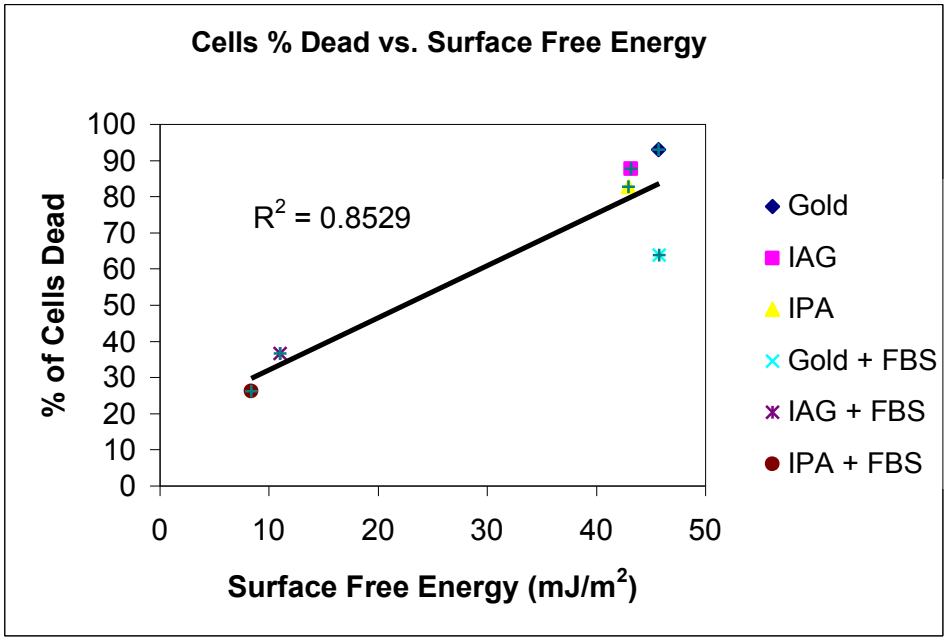

Figure 4.4 – Average Percent Dead Cells per Photo vs. Surface Free Energy. High R^2 value indicates strong correlation.

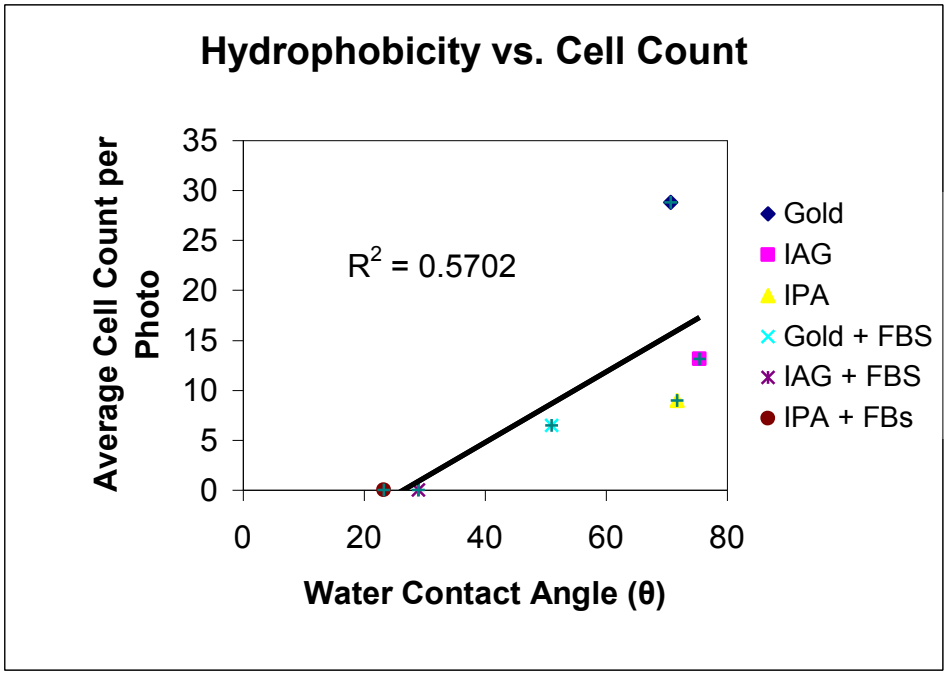

Figure 4.5 – Average Cell Count on Substrates per Photo vs. Hydrophobicity.

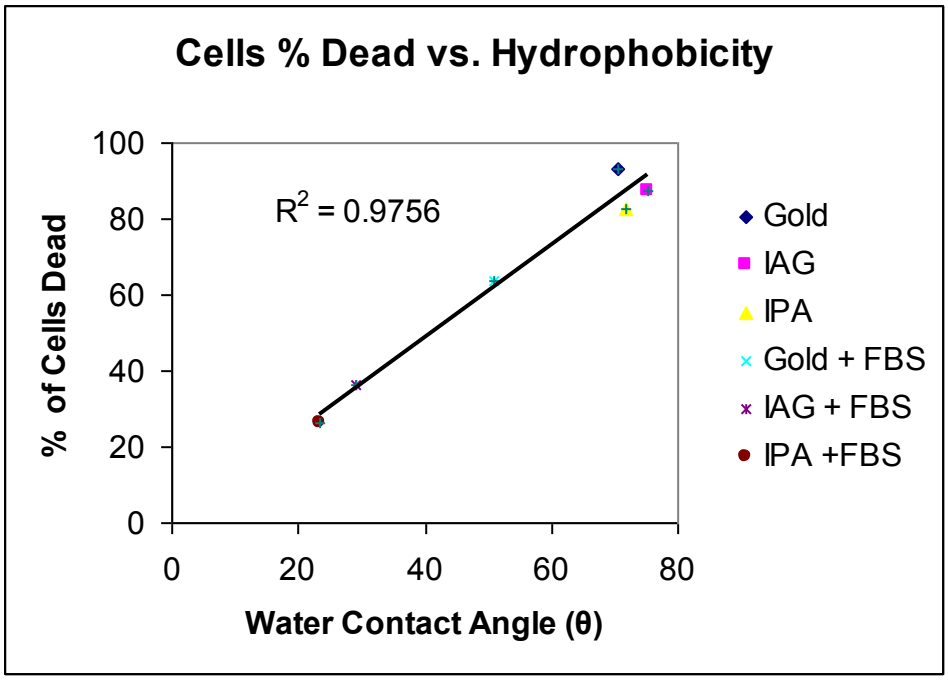

Figure 4.6 – Average Percent Dead Cells per Photo vs. Hydrophobicity. High R^2 value indicates strong correlation.

There was moderate correlation between total cells present per image and surface free energy and wettability. Many other factors important for cellular retention were not considered such as the zeta potential and surface roughness. Unexpectedly, there was strong correlation between surface free energies and hydrophobicity to viability. The greater hydrophobicity and surface free energy were, the lower the viability for *S. epidermidis*. Gottenbos *et al.* reported in their findings that adhesion of *S. epidermidis* to substrates was not affected by hydrophobicity. Instead, they reported that the more hydrophobic surfaces had the least bacterial growth. Although our studies did not examine bacterial growth on the various substrates, the more hydrophobic substrates

yielded the least number of viable bacteria, which would be consistent with their results. However, reasons for these phenomena are not understood.

4.4 – AFM

For protein adhesion experiments, concentrations of 100%, 50%, and 10% FBS were used to immerse gold slides for 80 minutes. After drying, the slides were imaged by AFM in air (Figure 4.7). Only 10% FBS can yield uniform structures. To confirm that the structures were not already present on gold, bare gold was also analyzed under the AFM. Bare gold had a very flat terrain, while FBS deposited gold substrates were wavy in appearance. The structures were completely different.

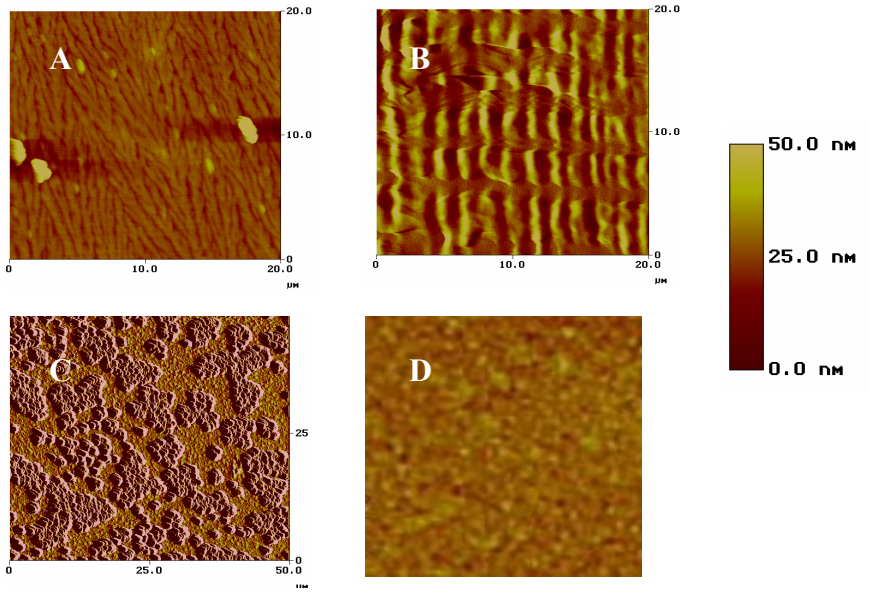

Figure 4.7 - Gold slides soaked in FBS solution. AFM photos taken were 512x512 pixels. Bar shows Z scale. (a) Gold substrate soaked in 10% FBS solution for 80 minutes (b) Gold substrate soaked in 50% FBS solution for 80 minutes (c) Gold substrate soaked in 100% FBS solution for 80 minutes (d) Bare gold

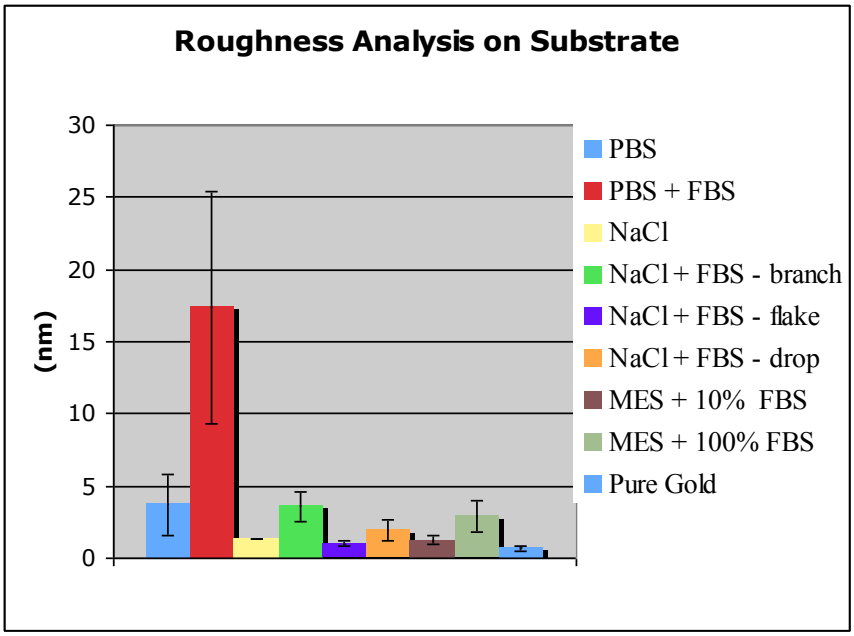

Figure 4.8 – AFM Roughness Analysis Compared to Gold Slides Soaked in Various Buffers

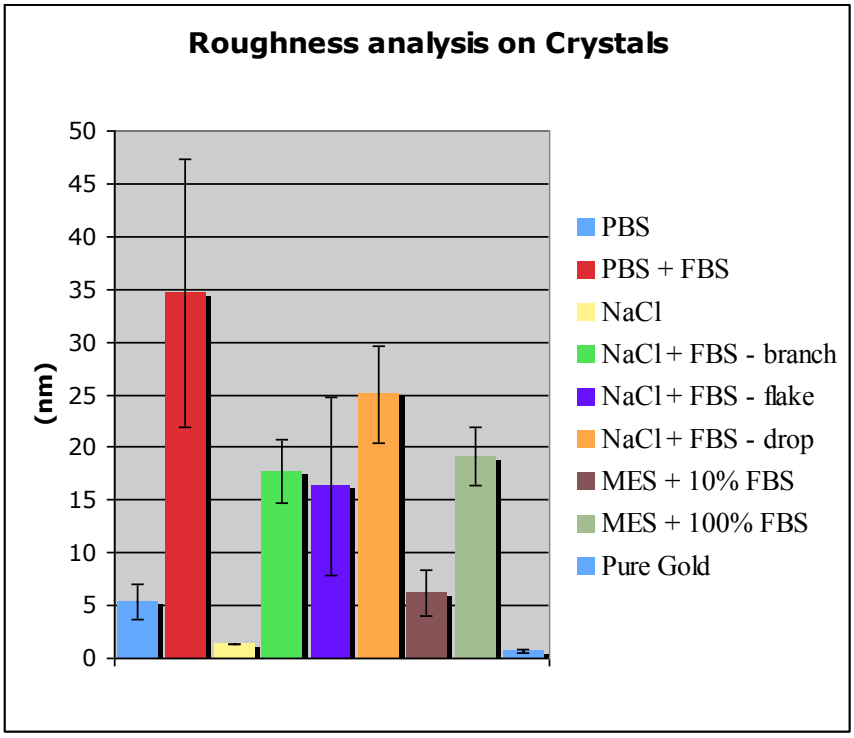

Figure 4.9 – Roughness Analysis on Crystals Formed by the Drying of Different Solutions on Gold

The data from Figures 4.8-9 indicate that pure gold and gold soaked in NaCl solution yielded substrates without deposits. The gold slide soaked in PBS + FBS exhibited the highest degree of deviation, with the height of crystal formation up to 35 nm. Considering the non-uniformity of the substrate, when sections of the slide towards the base were analyzed, roughness was generally below 5 nm, except for FBS + PBS. For crystal formations, different structures such as a branch or flake were analyzed separately. The results indicated little difference between buffer solutions and 0.1 M buffer solution was chosen for consistency with prior experiments.

4.5 – Bacterial Retention and Viability Experiments

The bacterial retention and viability experiments were carried out in two stages, without protein deposition and later with protein deposition. For each experiment with the live/dead kit, the information recorded for each picture included the date of

experiment, the concentration of cells in which the slide was submerged, the number of cells per image, the number of dead cells/image, the number of live cells/image, the percent dead, and the % alive. The substrate makeup such as glass, bare gold, IPA, IAG, PYR, TEG, or any combination with proteins were also recorded with each set of data (Tables 4.3-4).

Table 4.3 - Example of record keeping for an individual slide

S. epidermidis on bare gold 9.12.06					
Pic	Total	Dead	Live	% Dead	%Live
1	26	24	2	92.31	7.69
2	62	60	2	96.77	3.23
3	51	50	1	98.04	1.96
4	37	34	3	91.89	8.11
5	49	46	3	93.88	6.12
6	61	60	1	98.36	1.64
7	46	41	5	89.13	10.87
8	51	47	4	92.16	7.84
9	68	61	7	89.71	10.29
10	52	52	0	100.00	0.00
11	41	41	0	100.00	0.00
12	42	39	3	92.86	7.14
13	36	33	3	91.67	8.33
14	53	52	1	98.11	1.89
15	30	30	0	100.00	0.00
Average	47	45	2	94.99	5.01

Table 4.4 - Example of record keeping for all glass slides results

Glass Slides	Total	Dead	Live	% Dead	% Alive
1	3	0	3	0.00	100.00
2	4	2	2	41.46	58.54
3	6	1	5	17.24	82.76
4	19	15	4	77.04	22.96
5	8	1	6	18.11	81.89
6	13	2	11	18.81	81.19
7	1	0	1	0.00	100.00
8	3	0	3	0.00	100.00
9	3	0	3	0.00	100.00
10	4	1	3	17.68	82.32
11	10	1	9	12.37	87.63
12	9	0	9	1.42	98.58
13	8	5	3	67.27	32.73
14	6	3	3	53.71	46.29
15	13	9	4	65.97	34.03
Average	7	3	5	26.07	73.93
STDEV	5	4	3	27.60	27.60

It was decided that the slides would be soaked in bacterial solution for the 30 minute time interval so as to limit loss of viability due to starvation. For cell concentrations of 2×10^9 cells/mL on bare gold, the slide was saturated with bacteria. A 100X dilution was made to increase the accuracy of counting cells retained to the slides.

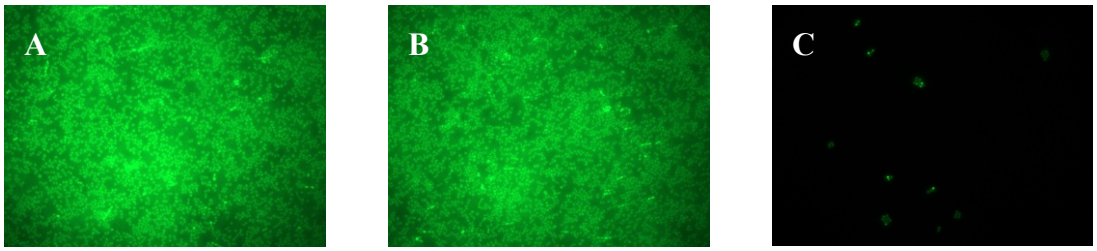

Figure 4.10 – Gold slides soaked in bacterial solutions. Area of 0.158 mm^2. (a) Gold slide soaked with 2 x 10^9 cells/mL overnight, approximately 14 hours (b) Gold slide soaked with 2 x 10^9 cells/mL for 1 hour (c) Gold slide soaked with 2 x 10^7 cell/mL for 30 minutes

For the first phase of the experiments, it was expected that the number of bacteria adhering to substrates such as IPA, IAG, and TEG would be the least. Previous research had suggested that TEG could prevent bacterial adhesion (Qian *et al.*, 2002). IPA and IAG were expected to result in the least bacterial retention because previous AFM experiments showed that the adhesion forces between *S. epidermidis* and these substrates were very low (Emerson, 2006). As for viability tests, no studies had been conducted between bacteria and the SAMs PYR, IPA, and IAG; thus it was not known how they would effect cell proliferation. However, IAG was expected to impact the viability since silver ions are toxic for bacteria (Chaw *et al.*, 2005).

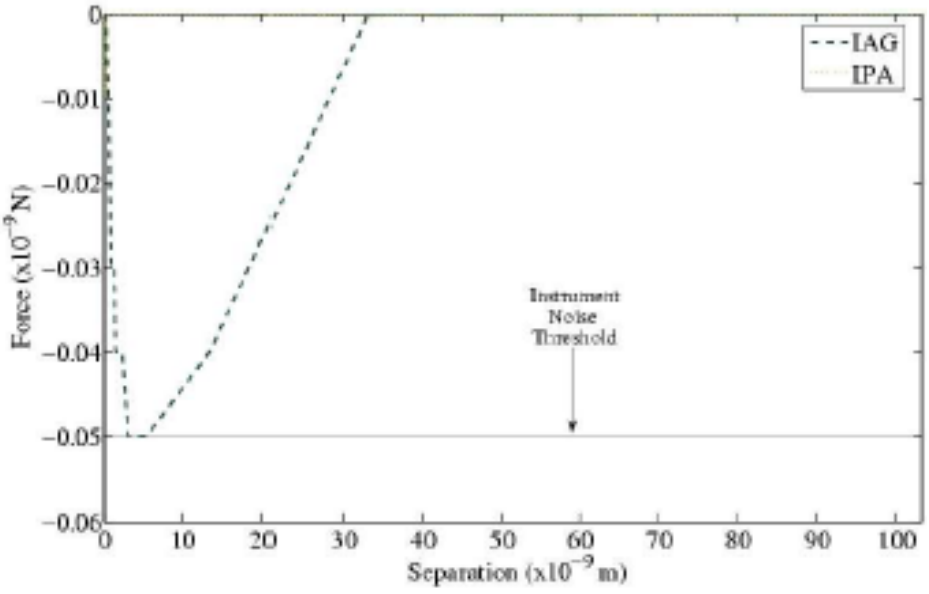

Figure 4.11 – Forces of adhesion measured between *S. epidermidis* and the Substrates IAG and IPA, using atomic force microscopy. The adhesion forces are below the instrument noise threshold, indicating that the interaction forces between these coatings and the bacteria on the AFM probe are very weak. Adapted from (Emerson, 2006).

The primary goal of the study was to limit the number of bacteria adhering to a substrate via chemical modification. A secondary goal was to observe if the SAMs also had any influence on the cell's viability. For each substrate, at least six slides were investigated. Remaining details may be found in Appendix A.

Substrates without adhered proteins:

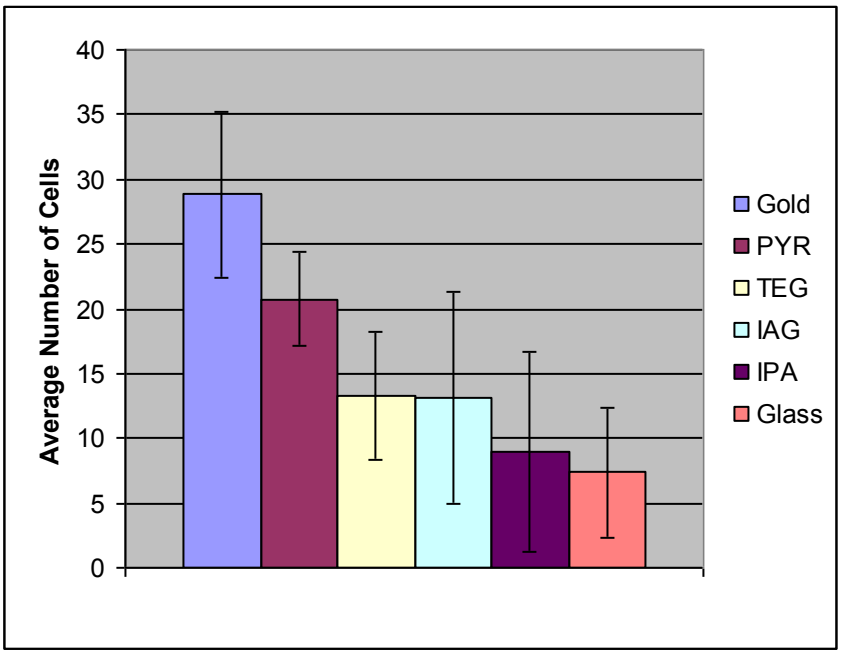

Figure 4.12 – Average Cell Counts per Photo (1000X) vs. Explored Substrates. Each photo has an area of 0.158 mm^2. Error bars represent standard deviations based on the average number of cells per photo on each slide. Results based on at least 6 replicates per substrate.

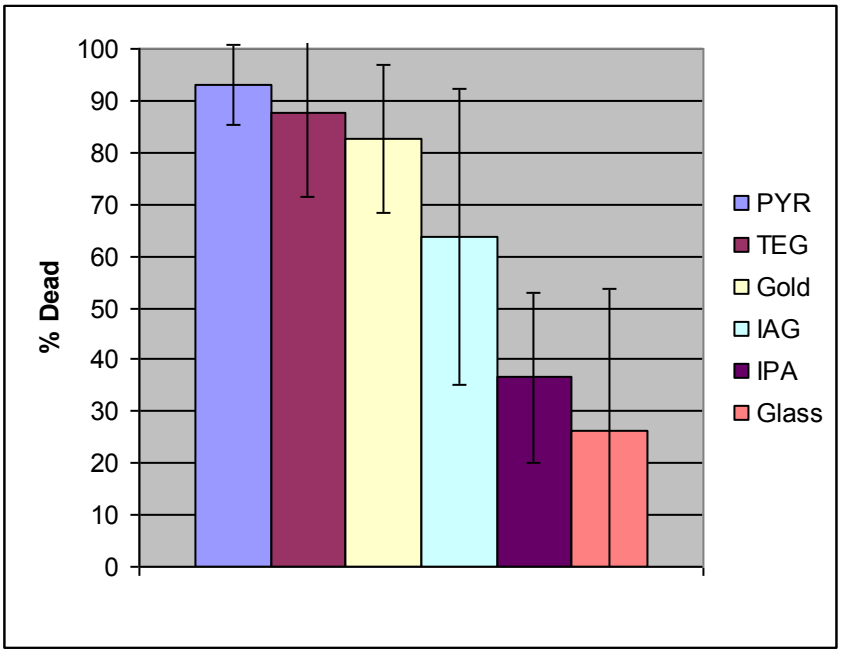

Figure 4.13 – Average Percent of Cells Fluorescing Red Under the Texas Red Filter. Each photo has an area of 0.158 mm^2. Error bars represent standard deviations based on the average percent dead cells per photo on each slide. Results based on at least 6 replicates per substrate.

The gold substrate exhibited the highest degree of cellular retention, while glass had the least, with 29 and 7 cells per frame on average, respectively (Figure 4.12). In terms of surface conditions such as hydrophobicity, both should have resulted in the same number of cells adhering. Glass and pure gold should be hydrophilic and have contact angles of < 30° (Abdelsalam *et al.*, 2005). However, in our experiments the gold substrate exhibited unusually high and variable contact angles ranging from 30° to 90°. It would be expected that the more hydrophobic a substrate is, the more likely hydrophobic bacteria are to adhere (Abdelsalam *et al.*, 2005). This indicates the *S. epidermidis* used for these experiments was hydrophobic.

SAMs terminating in TEG, IPA, and IAG were most anti-adhesive for the bacteria. They reduced bacterial retention by 54-69%, compared to gold. The PYR SAM

demonstrated moderate adhesive activity and did not exhibit a strong statistical difference from gold by conducting a one way analysis of variance (ANOVA) using the Sigma Stat software ($P>0.10$). Previous experiments with TEG found little or no bacteria adhering in similar experiments (Qian *et al.*, 2002).

Our unexpected results may be explained by the non-uniform nature of TEG on the substrates, based on AFM studies from our laboratory (Figure 4.14) (Emerson, 2006). For self-assembled monolayers we would expect a smoother substrate. IPA and IAG formed uniform substrates (Figure 4.14).

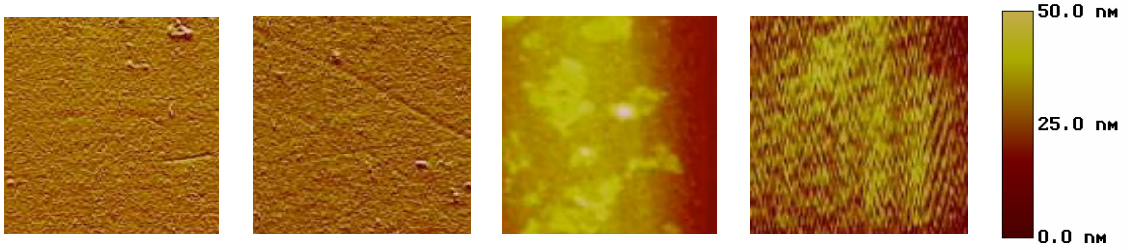

Figure 4.14 – AFM Images, from left to right, of IAG, IPA, TEG, and PYR. Pictures are 25 μm^2 in scan area with 256 x 256 pixels per image. Bar shows Z scale. Adapted from (Emerson, 2006)

When cell proliferation was considered, bare gold, PYR, and TEG were most effective against cell viability (Figure 4.13). The results between the three were statistically similar by conducting an ANOVA test ($P>0.10$). In these cases on average between 83-93% of the cells were found fluorescing red under the Texas Red filter, suggesting they were dead. For IPA and IAG fewer adhered cells were dead, with average dead cell percentages of 36% and 64%, respectively. This represented a statistical difference between SAMs ($P<0.05$). Of all the SAMs, IAG was expected to be most effective against cell viability due to the addition of the silver ions. The addition of silver ions made IAG more effective against cell proliferation than IPA, even though the

mechanism is not completely understood at this time. For gold, PYR, and TEG, there was no statistical difference between the three, with the differences due to random sampling variability ($P>0.10$).

Substrates Coated with FBS:

Studying the interactions between the bacteria and the SAMs helps us to understand fundamental interactions between bacteria and different types of chemically-modified surfaces. However, in order to be useful for an *in vivo* situation, the behavior of the SAMs should be investigated in the presence of proteins, since these compounds will naturally be present in the bloodstream and could interfere with the anti-adhesive or antimicrobial action of the SAM. Probably more important to consider is the effect, if any, SAMs have on bacterial adhesion and viability when proteins adhere to a substrate. When a catheter is placed in the body, proteins begin accumulating on the substrate immediately after it enters the bloodstream (Leid *et al.*, 2002). For the SAMs to be useful for a patient, they must alter the protein layer or interact with the bacteria. For these studies, gold covered with FBS was the control group. We chose FBS because it can be a useful model for non-specific binding between bacteria and proteins.

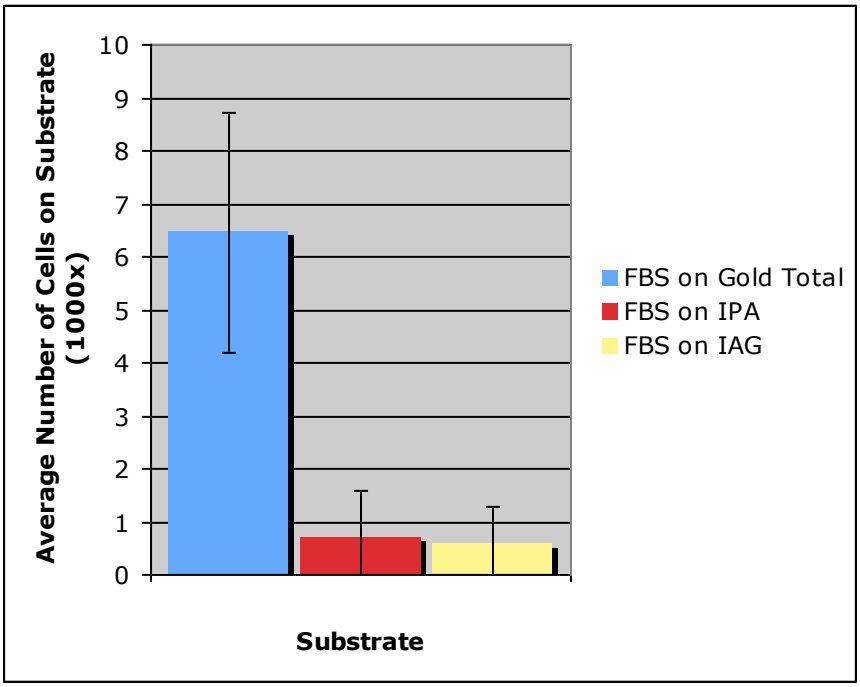

Figure 4.15 - Average Cell Counts per Photo (1000X) vs. FBS Coated Substrates. Each photo has an area of 0.158 mm^2. Error bars represent standard deviation based on the average number of cells per photo on each slide. Results based on at least 5 replicates per substrate.

When FBS was adsorbed to the bare gold, the total cell count was dramatically reduced (Figure 4.15). Compared to bare gold, FBS-covered gold resulted in a reduction of bacterial retention by 75%. It was expected for *S. epidermidis* that the number of cells adhering would be reduced due to work from previous studies (Murga *et al.*, 2001). Previous results demonstrated that submerging slides in 10% FBS solution for 80 minutes completely altered the surface chemistry. There was also a large difference between the protein deposited substrates and substrates without proteins in terms of cell viability for our study.

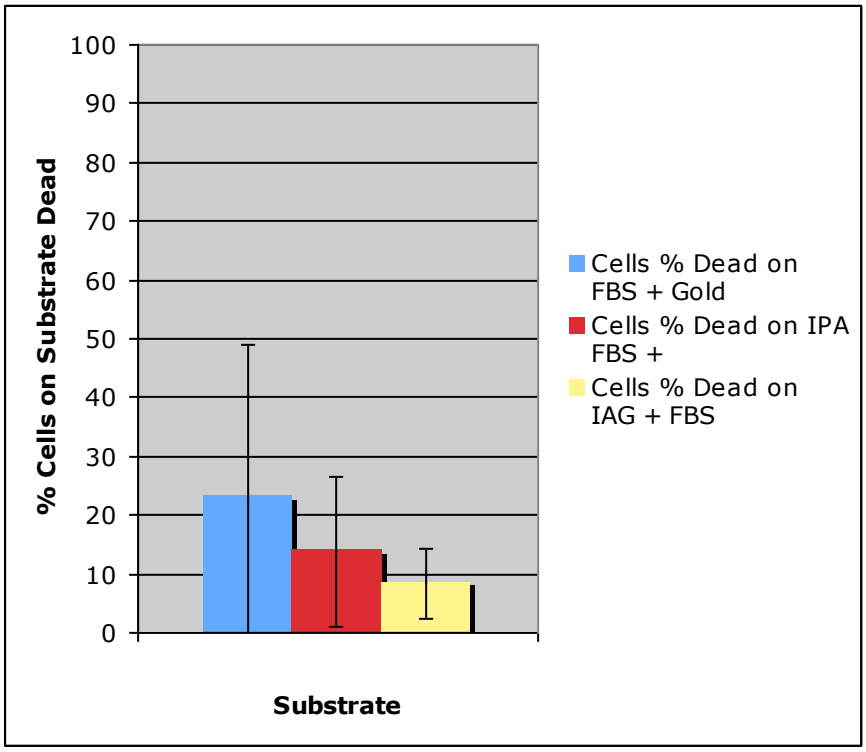

Figure 4.16 - Average Percent of Cells Fluorescing Red Under the Texas Red Filter on FBS Coated Substrates. Error bars represent standard deviations based on the average percent dead cells per photo on each slide. Results based on at least 5 replicates per substrate.

For the FBS covered gold, 23% of the cells were dead, compared to the bare gold with 83% dead (Figure 4.16). The increase of cell proliferation when proteins are present may explain why *S. epidermidis* can cause horrible infections in patients, since only one culturable cell is necessary to initiate the biofilm.

When IAG and IPA were considered with FBS, results consistently demonstrated that the number of retained bacteria on the slides was reduced close to zero and statistically different over SAMs without FBS ($P<0.05$). This is an indication that the alterations in surface chemistry impact bacterial retention, even though proteins coated the surface. There appears to be an increase in cell viability for bacteria on these substrates as well. Very few bacteria were found on these substrates, making any

significance in terms of viability difficult to characterize. On the IPA + FBS slide, viability increased by 62% over bare IPA. For the IAG slide, cell viability increased by 86% over bare IAG. Both changes were statistically significant over SAMs without adsorbed FBS ($P<0.05$). Although the results of these experiments show that cell viability increases, considering cellular retention reduced nearly to zero, these SAMs are promising to preventing CRBSIs.

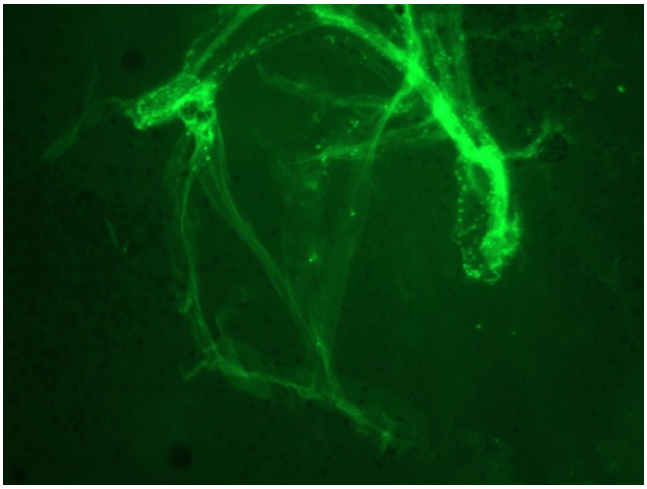

Figure 4.17 – Picture of FBS on IPA Slide. Photo taken under a FITC filter.

5.0 – Conclusions

5.1 – Generalizations Based on Experimental Results

The goal of this project was to observe changes in *S. epidermidis* retention and viability on substrates due to the presence of SAMs. A series of SAMs were employed, which differed in the terminal functional group that is exposed to the bacterium or protein. The terminal groups of the SAMs tested were 4-(16-bromo hexadecyloxy)pyridine (PYR), (1-Mercaptounec-11-yl)tri(ethylene glycol) (TEG), 5-(10-mercaptodecyloxy)-isophthalic acid (IPA), and isophthalic acid with silver (IAG). The retention and viability of *S. epidermidis* to each of these surfaces were quantified using a dual staining technique that allowed for the distinguishing between live and dead cells, namely propidium iodide and Syto 9. For bare gold, and the IAG and IPA terminating SAMs, FBS was adsorbed to the substrates to further mimic *in vivo* conditions. Microbial retention on the slides was analyzed using fluorescence microscopy, employing a 100X objective lens FITC and Texas Red filters, and the Spot Advanced computer software. Mechanisms of adhesion were also analyzed by calculating the surface free energy and hydrophobicity of the varying substrates.

Bacterial retention was always reduced when the cells were exposed to SAM coated surfaces. IAG, IPA, and TEG were most effective coatings, with the greatest ability to decrease bacterial retention. In terms of viability, PYR bare gold, and TEG were comparable and resulted in the lowest degree of cell viability. Some changes could be observed in cellular retention upon the introduction of protein, confirming that experiments designed to mimic *in vivo* conditions must always assess the effects of proteins along with the bacteria. On gold + FBS substrates, cellular retention was

moderate, while IPA and IAG + FBS substrates resulted in almost no detectable bacteria on the surfaces. These results are consistent with the reduction of surface free energy when protein is present.

IPA and IAG show promise for reducing biofilm formation on catheters or other biomaterials due to *S. epidermidis*. The reduction in retention when FBS is present is a very important part of this finding. Reduction in surface free energy explains the change in bacterial retention, but may not be absolutely appropriate to describe adhesion characteristics in all cases. On substrates without FBS present, exposure to all of the SAMs decreased retention, even though large variations in the surface free energies could not be observed. Quantifying adhesion characteristics in simple algorithms may not be suitable as of yet, but understanding the effect that different physicochemical parameters, such as surface roughness, hydrophobicity, and surface free energy, have on bacterial retention and viability can potentially be useful in a number of future applications.

5.2 – Future Recommendations

Further work can be carried with FBS on TEG and PYR to see if the results are similar to those of IAG and IPA. It is important to consider the effects of testing these SAMs with other proteins that can mimic *in vivo* conditions. Many more researchers use fibronectin to compare laboratory experiments to *in vivo* conditions. Only when results from these studies are concluded should there be any consideration for actual *in vivo* experiments. Results from the live/dead kit should continue to be verified since the kit only indicates the state of the cell membrane and does not truly describe a metabolic function, such as cell respiration. Finally, these experiments dealt with only one strain of *S. epidermidis*. Although a clinical isolate, it would be advantageous to test the SAMs

against other strains to ensure their effectiveness against the various forms of *S. epidermidis* found in nosocomial cases.

6.0 - Sources

Abdelsalam, M. E., Bartlett, P. N., Kelf, T. and Baumberg, J. 2005. **Wetting of Regularly Structured Gold Surfaces**. *Langmuir; 21: 1753-1757*

Absolom, D. R., Lamberti, F. V., Policova, Z., Zingg, W., van Oss, C. J., and Neumann, A. W. 1983. **Surface Thermodynamics of Bacterial Adhesion**. *Applied and Environmental Microbiology; 46: 90-97*

Abu-Lail, N. I. and Camesano, T. A. 2006. **Specific and Nonspecific Interaction Forces Between *Escherichia coli* and Silicon Nitride, Determined by Poisson Statistical Analysis**. *Langmuir, in press*.

An, Y. H. and Friedman, R. J. 1997. **Concise Review of Mechanisms of Bacterial Adhesion to Biomaterial Surfaces**. *Journal Biomedical Materials Resources; 43: 338-348*

Atomic Force Microscopy. *David B.; California Institute of Technology*. http://www.stm2.nrl.navy.mil/how-afm/how-afm.html (6.1.06)

Atomic Force Microscopy. *Simon H.; University of Bristol* http://spm.phy.bris.ac.uk/techniques/AFM/ (6.1.06)

Banning, N., Toze, S., and Mee, B. J. 2002. ***Escherichia coli* survival in groundwater and effluent measured using a combination of propidium iodide and the green fluorescent protein.** *Journal of Applied Microbiology; 93: 69-76*

Bigelow, W. C., Pickett, D. L., and Zisman, W. A. J. 1946. **Colloid Interface.** *Science; 1: 513.*

Biofilm - Key to understanding and controlling bacterial growth in Automated Drinking Water Systems. *Edstrom Industries, Inc.* http://www.edstrom.com/Resources.cfm?doc_id=23 (6.1.06)

Boulus, L., Prévost, M., Barbeau, B., Coallier, J., and Desjardins, R. 1999. **Live/Dead BacLight™: application of a new rapid staining method for direct enumeration of viable and total bacteria in drinking water.** *Journal of Microbiological Methods; 37: 77-86*

Burnham, N. A., Chen, X., Hodges, C. S., Matei, G. A., Thoreson, E. J., Roberts, C. J., Davies, M. C., and Tendler, S. J. B.. 2003. **Comparison of calibration methods for atomic-force microscopy cantilevers**. *Institute of Physics Publishing; 14: 1-6*

Busscher, H. J., Weekamp, A. H., van der Mei, H. C., van Pelt, A. W. J., de Jong, H. P., and Arends, J. 1984. **Measurement of the Surface Free Energy of Bacterial Cell Surfaces and Its Relevance for Adhesion**. *Applied and Environmental Microbiology*; *48: 980-983*

Central Venous Catheters. ©2005 WebMD, Inc. http://www.webmd.com/hw/health_guide_atoz/tp21279.asp (12.9.05)

Chaw, K.C., Manimaran, M., and Tay, F. E. H. 2005. **Silver Ions and *S. epidermidis* Biofilm Destabilization.** *Antimicrobial Agents and Chemotherapy; 49: 4853-4859*

Darouiche, R., Wright, C., Hamill, R., Koza, M., Lewis, D., and Markowski, J. 1991. **Eradication of Colonization by Methicillin-Resistant *S. aureus* by Using Oral Minocycline-Rifampin and Topical Mupirocin.** *Antimicrobial Agents and Chemotherapy; 35: 1612-1615*

Depuydt, S. I. B. P., Annemans, L., Benoit, D., Hoste, E., De Waele, J. J., Decruyenaere, J., Vogelaers, D., Colardyn, F., and Vandewoude, K. H.. 2005. **Clinical and**

Economic Outcomes in Critically Ill Patients with Nosocomial Catheter-Related Bloodstream Infections. *Clinical Infectious Diseases; 41:1591–8*

Emerson, R. 2006. **A Nanoscale Investigation of Microbial Adhesion to Biomedical Implant Devices**. *Worcester Polytechnic Institute*.

Foster, T. ***S.* epidermidis**. http://gsbs.utmb.edu/microbook/ch012.htm (12.9.05)

Gallardo-Moreno, A. M., Gonzalez-Martin, M. Luisa, B., Jose M., Perez-Giraldo, C., and Gomez-Garcia, A. C. 2002. **Serum as a Factor Influencing Adhesion of Entercoccus faecalis to Glass and Silicone**. *Applied and Environmental Microbiology; 68: 5784-5787*

Gallardo-Moreno, A. M., Gonzalez-Marin, M. L., Bruque, J. M., and Perez-Giraldo, C. 2004. **Changes on the physico-chemical surface properties and adhesion behaviour of Enterococcus faeclis by the addition of serum or urine to the growth medium.** *Physical Chemistry Chemical Physics; 7: 1620-1631*

Giesbrecht, P., Kersten, T., Maidhof, H., and Wecke, J. 1998. **Staphylococcal Cell Wall: Morphogenesis and Fatal Variations in the Presence of Penicillin**. *Microbiological and Molecular Biology Reviews; 62: 1371-1414*

Gottenbos, B., van der Mei, H. C, Busscher, H. J. 1999. **Initial adhesion and surface growth of *S. epidermidis* and *Pseudomas aeruginosa* on biomedical polymers.** *Journal Biomedical Materials Resources; 50: 208-214*

Gu, J., Li, H., Li, M., Vuong, C., Otto, M., Wen, Y., Gao, Q. 2005. **Bacterial Insertion Sequence IS*256* as a Potential Molecular Marker to Discriminate Invasive Strains from Commensal Strains of *S. epidermidis*.** *Journal of Hospital Infection; 61: 342-348*

Gudehus, G. **Gleichgewichts-, Umlagerungs- und Transportphänomene bei Peloiden** http://www.rz.uni-karlsruhe.de/~gn43/DLVO.JPG (7.11.06)

Heparin Sodium Injection, USP. Copyright 2005 by RxList, Inc. http://www.rxlist.com/cgi/generic/heparin.htm (11.30.05)

Hu, J. and Fox, M. A. 1999. **A convenient trimethylsilylthioxy-dehalogenation reaction for the preparation of functionalized thiols.** *Journal of Organic Chemistry; 64: 4959-4691*

Hume, E.B.H., J. Muir, Baveja, B., Schubert, T.L., Kumar, N., Kjelleberg, S., Griesser, H.J., Thissenf, H., Read, R., Poole-Warren, L.A., Schindhelm, K., Willcox, M.D.P. 2004. **The control of *S.* epidermidis biofilm formation and in vivo infection rates by covalently bound furanones.** *Biomaterials; 2: 5023–5030*

Israelachvili, J. Intermolecular and Surface Forces. *Academic Press, Inc., CA. 1992, 2nd edition*.

Ista, Linnea K., Fan, Hongyou, Oswald, Baca, López, Gabriel P. 1996. **Attachment of bacteria to model solid surfaces oligo(ethylene glycol) surfaces inhibit bacterial attachment**. *FEMS Microbiology Letters; 142: 59-63*

Keer, J. T. and Birch, L. 2003. **Molecular Methods for the Assessment of Bacterial Viability.** *Journal of Microbiological Methods; 53: 175-183*

Kinraide, T. B. 1994. **Use of a Gouy-Chapman-Stern Model for Membrane-Surface Electrical Potential to Interpret Some Features of Mineral Rhizotoxity**. *Plant Physiology; 106: 1583-1592*

Kloos, W. E. and Bannerman, T. L. **Update on Clinical Significance of Coagulase-Negative Staphylococci**. 1994. *Clinical Microbiology Reviews; 7: 117-140*

Leid, J. G., Shirtliff, M. E., Costerton, J. W., and Stoodley, P. 2002. **Human Leukocytes Adhere to, Penetrate, and Respond to *S.* aureus.** *Infection and Immunity; 70: 6339–6345.*

McLaughlin, S. 1989. **The Electrostatic Properties of Membranes**. *Annual Reviews; 18: 113-36*

Mermel, L. A. 2001**. New Technologies to Prevent Catheter-Related Bloodstream Infections Intravascular.** *Emerging Infectious Diseases Vol. 7, No. 2*

MikroMasch. http://www.spmtips.com/products/cantilevers/catalog/ (6.13.06)

Morales, Manuel, Mendez-Alvarez, Sebastian, Mart, Juana-Victoria, Marrero, Carmen, and Freytes, Cesar O. 2004. **Biofilm: the microbial "bunker" for intravascular catheter-related infection.** *Support Care Cancer; 12: 701–707*

Murga, R., Miller, J. M., Donlan, R. M. 2001. **Biofilm Formation by Gram-Negative Bacteria on Central Venous Catheter Connectors: Effect of Conditioning Films in a Laboratory Model.** *Journal of Clinical Microbiology; 39: 2294–2297*

Pale-Grosdemange, C., Simon, E. S., Prime, K. L., and Whitesides, G. M. 1991. **Formation of self-assembled monolayers by chemisorption of derivatives of oligo(ethylene glycol) of structure HS(CH2)11(OCH2CH2)mOH on gold.** *Journal of the American Chemical Society; 113: 12-20*

Plummer, S. T., Wang, Q., and Bohn, P. W. 2003. **Electrochemically Derived Gradients of the Extracellular Matrix Protein Fibronectin on Gold.** *Langmuir; 19: 7528-7536*

Prescott, L. M., Harley, J. P., and Klein, D. A. Microbiology. *McGraw Hill. 2005. 6th edition*.

Qian, X., Metallo, S. J., Choi, I. S., Wu, H., Lia, M. N., and Whitesides, G. M. 2002. **Arrays of Self-Assembled Monolayers for Studying Inhibition of Bacterial Adhesion.** *Anal. Chem; 74: 1805-1810*

Ryder, M. A. 2005. **Catheter-Related Infections: It's All About Biofilm.** *Topics in Advanced Practice Nursing eJournal; 5: 3*

Sampath L., Tambe S., and Modak S. 1999. **Comparison of the efficacy of antiseptic and antibiotic catheters impregnated on both their luminal and outer surfaces**. *Programs and Abstracts of the 39th Interscience Conference on Antimicrobial Agents and Chemotherapy*

Schmitt, S. K., Knapp, C., Hall, G. S., Longworth, D. L., McMahon, J. T., and Washington, J. A. 1998. **Impact of Chlorhexidine–Silver Sulfadiazine-Impregnated Central Venous Catheters on In Vitro Quantitation of Catheter-Associated Bacteria.** *Journal of Clinical Microbiology; 34: 2640-2641*.

Shah, C. B., Mittelman, M. W., Costerton, J. W., Parenteau, S., Pelak, M., Arsenault, R., and Mermel, L. A.. 2002. **Antimicrobial Activity of a Novel Catheter Lock Solution.** *Antimicrobial Agents and Chemotherapy; 46: 1674–1679*

Simon, A. and Durrieu, M.-C. 2006. **Strategies and results of atomic force microscopy in the study of cellular adhesion.** *Micron; 37: 1-13*

Soto, E. R., MacDonald, J. C., Cooper, C. G. F., and McGimpsey, W. G. 2003. **A non-covalent strategy for the assembly of supramolecular photocurrent-generating systems.** *Journal of the American Chemical Society; 125: 2838-2839*

Taurolock™. TauroPharm GmbH. http://www.tauropharm.de/TauroLock.html (12.9.05)

The Nobel Prize in Physics: 1986. *The Nobel Foundation.* http://nobelprize.org/physics/laureates/1986/index.html (6.1.06)

Turgut, H., Sacar, S., Kaleli, I., Sacar, M., Goksin, I., Toprak, S., Asan, A., Cevahir, N., Tekin, K., and Baltalarli, A. 2005. **Systemic and local antibiotic prophylaxis in the prevention of *S.* epidermidis graft infection.** *BMC Infectious Diseases; 5: 91-94*

Ulman, A. 1996. **Formation and Structure of Self-Assembled Monolayers.** *Chemistry Review; 96: 1533-1554*

van Loosdrecht, M. C. M., Lyklema, J., Norde, W., Schraa, G., and Zehnder, A. J. B.. 1987. **The Role of Bacterial Cell Wall Hydrophobicity in Adhesion**. *Applied and Environmental Microbiology*; *53: 1893-1897*

Zhou, Y., Doerschuk, C. M. Anderson, J. M., Marchant, R. E. 2004. **Biomaterial surface-dependent neutrophil mobility.** *Journal of Biomedical Materials; 69: 611-620*

7.0 – Appendices

Appendix A - Tables of Results for Live/Dead Kit

Table 7.1 – Adhesion to Bare Substrates

Gold Slides	Average Total	Dead	Live	% Dead	% Alive
1	33.60	24.13	9.47	71.82	28.18
2	33.80	21.67	12.13	64.11	35.89
3	26.33	19.87	6.46	75.47	24.53
4	23.33	22.67	0.66	97.17	2.83
5	23.93	20.67	3.26	86.38	13.62
6	30.93	14.27	16.66	46.14	53.86
7	27.60	26.93	0.67	97.57	2.43
8	19.53	18.67	0.86	95.60	4.40
9	24.87	19.27	5.60	77.48	22.52
10	47.00	44.67	2.33	95.04	4.96
11	32.73	25.53	7.20	78.00	22.00
12	26.07	22.27	3.80	85.42	14.58
13	27.07	25.27	1.80	93.35	6.65
14	29.00	25.87	3.13	89.21	10.79
15	26.47	23.27	3.20	87.91	12.09
Average	28.82	23.67	5.15	82.71	17.29
STDEV	6.42	6.69	4.61	14.28	14.28
Glass Slides	Average Total	Dead	Live	% Dead	% Alive
1	3	0	3	0.00	100.00
2	4	2	2	41.46	58.54
3	6	1	5	17.24	82.76
4	19	15	4	77.04	22.96
5	8	1	6	18.11	81.89
6	13	2	11	18.81	81.19
7	1	0	1	0.00	100.00
8	3	0	3	0.00	100.00
9	3	0	3	0.00	100.00
10	4	1	3	17.68	82.32
11	10	1	9	12.37	87.63
12	9	0	9	1.42	98.58
13	8	5	3	67.27	32.73
14	6	3	3	53.71	46.29
15	13	9	4	65.97	34.03
Average	7	3	5	26.07	73.93
STDEV	5	4	3	27.60	27.60
IPA Slides	Average Total	Dead	Live	% Dead	% Alive
1	8.87	1.27	7.60	14.32	85.68
2	10.07	2.27	7.80	22.54	77.46
3	27.47	8.13	19.34	29.60	70.40
4	3.40	0.93	2.47	27.35	72.65

5	4.00	1.40	2.60	35.00	65.00
6	1.73	0.53	1.20	30.64	69.36
7	11.20	7.27	3.93	64.91	35.09
8	4.00	2.07	1.93	51.75	48.25
9	10.07	5.27	4.80	52.33	47.67
Average	8.98	3.24	5.74	36.49	63.51
STDEV	7.77	2.88	5.62	16.38	16.38
IAG Slide	Average Total	Dead	Live	% Dead	% Alive
1	22.2	21.93	0.27	98.78	1.22
2	10.8	4.13	6.67	38.24	61.76
3	10.6	4.2	6.4	39.62	60.38
4	22.07	8.13	13.93	36.84	63.16
5	12.67	10.6	2.33	83.66	16.34
6	0.47	0.4	0.13	85.11	14.89
Average	13.14	8.23	4.96	63.71	36.29
STDEV	8.18	7.59	5.25	28.42	28.42
PYR Slide	Average Total	Dead	Live	% Dead	% Alive
1	18	18	0	100.00	0.00
2	20.53	20.46	0.07	99.66	0.34
3	26.53	25.13	1.4	94.72	5.28
4	23.6	20.53	3.07	86.99	13.01
5	18	14.53	3.47	80.72	19.28
6	17.87	17.13	0.73	95.86	4.14
Average	20.76	19.30	1.46	92.99	7.01
STDEV	3.61	3.63	1.50	7.63	7.63
TEG slide	Average Total	Dead	Live	% Dead	% Alive
1	12.80	12.53	0.27	97.89	2.11
2	15.87	10.20	5.67	64.27	35.73
3	21.67	20.93	0.73	96.59	3.41
4	12.00	12.00	0.00	100.00	0.00
5	8.40	5.80	2.60	69.05	30.95
6	9.07	8.87	0.20	97.79	2.21
Average	13.30	11.72	1.58	87.60	12.40
STDEV	4.91	5.12	2.22	16.33	16.33

Table 7.2 – Adhesion to Substrates with Deposited FBS

Phase II compiled results.			GOLD + FBS			
		Total	Dead	Live	% Dead	% Live
4.12.06	1.00	7.93	3.33	4.60	42.02	57.98
	2.00	4.07	2.40	1.67	59.02	40.98
4.19.06		4.47	0.27	4.20	5.97	94.03
4.26.06		6.31	0.38	5.94	5.94	94.06
6.16.06		9.40	0.33	9.07	2.70	97.30
Average		6.44	1.34	5.09	23.13	76.87
STDEV		2.27	1.43	2.71	25.75	25.75
			IPA + FBS			
		Total	Dead	Live	% Dead	% Live
6.12.06		1.20	0.13	1.07	25.00	75.00
6.21.06		0.20	0.00	0.20	0.00	100.00
6.30.06		0.00	0.00	0.00	NA	NA
7.10.06 (a)		2.00	0.27	1.60	16.67	83.33
(b)		0.00	0.00	0.00	0.00	0.00
Average		0.68	0.08	0.57	13.89	86.11
STDEV		0.89	0.12	0.72	12.73	12.73
			IAG + FBS			
		Total	Dead	Live	% Dead	% Live
6.21.06		0.00	0.00	0.00	NA	NA
6.30.06		0.20	0.00	0.20	NA	NA
7.11.06 (a)		0.53	0.07	0.47	12.58	88.04
(b)		1.60	0.07	1.53	4.17	95.81
Average		0.58	0.03	0.55	8.38	91.93
STDEV		0.71	0.04	0.68	5.95	5.50

Appendix B – Table of Results for Contact Angles

Table 7.3 – Contact Angles on Substrates w/o FBS

	Left						
	X	Y	R	arcSin	arcCos	average	Error check
Uncleaned gold W	2.30	0.05	2.35	78.16	88.78	83.47	0.96
	///	///	///	90.00	90.00	90.00	1.00
	///	///	///	90.00	90.00	90.00	1.00
	///	///	///	90.00	90.00	90.00	1.00
D	4.00	6.90	8.00	30.00	30.40	30.20	0.99
	3.95	7.40	8.40	28.05	28.24	28.15	1.00
	4.10	8.45	9.50	25.57	27.19	26.38	0.98
F	28.00	9.50	29.50	71.65	71.21	71.43	1.00
	2.50	1.50	2.90	59.55	58.85	59.20	1.01
	2.85	0.90	3.00	71.81	72.54	72.17	0.99
	2.43	1.20	2.70	63.92	63.61	63.76	1.00
	2.55	1.60	3.05	56.73	58.36	57.54	0.97
	3.05	1.30	3.30	67.55	66.80	67.18	1.01
Clean gold W	2.15	1.05	2.45	61.35	64.62	62.99	0.95
	2.20	0.70	2.30	73.04	72.28	72.66	1.01
	2.05	0.55	2.15	72.46	75.18	73.82	0.97
	2.20	0.85	2.40	66.44	69.26	67.85	0.97
D	4.00	22.00	23.00	10.02	16.96	13.49	0.95
	3.25	8.75	9.35	20.34	20.64	20.49	1.00
	3.55	12.90	13.35	15.42	14.92	15.17	1.00
	3.35	11.85	12.30	15.80	15.55	15.68	1.00
F	2.35	1.45	2.85	55.54	59.42	57.48	0.94
	2.40	1.45	2.80	59.00	58.81	58.90	1.00
IPA W	1.83	0.75	2.00	65.85	67.98	66.91	0.97
	2.90	1.15	3.15	67.02	68.59	67.80	0.98
	1.75	0.35	1.80	76.46	78.79	77.63	0.98
	2.70	1.40	3.10	60.57	63.15	61.86	0.96
D	2.93	6.00	6.60	26.31	24.62	25.46	1.02
	3.00	6.40	7.10	24.99	25.66	25.33	0.99
F	3.75	4.10	5.60	42.04	42.93	42.49	0.98
	2.33	1.95	3.05	49.67	50.26	49.96	0.99
	2.38	1.70	3.00	52.34	55.48	53.91	0.95
IAG W	1.75	0.40	1.80	76.46	77.16	76.81	0.99
	1.80	0.40	1.85	76.65	77.51	77.08	0.99
	1.70	0.45	1.75	76.27	75.10	75.69	1.01
	1.78	0.60	1.90	69.10	71.59	70.35	0.97
D	2.93	5.00	5.90	29.72	32.06	30.89	0.96
	2.83	6.30	7.00	23.80	25.84	24.82	0.97
F	2.35	1.70	2.90	54.13	54.11	54.12	1.00
	3.30	2.70	4.20	51.79	49.99	50.89	1.03
	2.13	1.50	2.60	54.82	54.77	54.79	1.00
	3.70	3.30	5.00	47.73	48.70	48.22	0.98

	Right					Error		
X	Y	R	arcSin	arcCos	average	check	Overall Average	
///	///	///	90.00	90.00	90.00	1.00	**86.74**	**89.18**
///	///	///	90.00	90.00	90.00	1.00	**90.00**	**1.63**
///	///	///	90.00	90.00	90.00	1.00	**90.00**	
///	///	///	90.00	90.00	90.00	1.00	**90.00**	
4.00	6.90	8.00	30.00	30.40	30.20	0.99	**30.20**	**28.58**
3.95	7.40	8.40	28.05	28.24	28.15	1.00	**28.15**	**1.45**
4.10	7.60	8.65	28.29	28.52	28.41	1.00	**27.39**	
28.00	10.00	30.00	68.96	70.53	69.74	0.98	**70.59**	**65.45**
2.50	1.10	2.70	67.81	65.96	66.88	1.02	**63.04**	**3.60**
2.85	0.90	3.00	71.81	72.54	72.17	0.99	**72.17**	**OUT**
2.43	1.20	2.75	61.86	64.13	63.00	0.97	**63.38**	
2.55	1.10	2.75	68.01	66.42	67.22	1.02	**62.38**	
3.05	1.25	3.25	69.79	67.38	68.59	1.03	**67.88**	
2.15	0.90	2.40	63.62	67.98	65.80	0.94	**64.39**	**70.67**
2.20	0.70	2.30	73.04	72.28	72.66	1.01	**72.66**	**4.80**
2.05	0.45	2.10	77.47	77.63	77.55	1.00	**75.68**	
2.20	0.75	2.30	73.04	70.97	72.01	1.02	**69.93**	
4.00	22.00	23.00	10.02	16.96	13.49	0.95	**13.49**	**16.09**
3.25	9.35	9.85	19.27	18.33	18.80	1.01	**19.64**	**2.57**
3.55	12.10	12.55	16.43	15.39	15.91	1.01	**15.54**	
3.35	11.85	12.30	15.80	15.55	15.68	1.00	**15.68**	
2.35	1.30	2.70	60.50	61.22	60.86	0.99	**59.17**	**59.04**
2.40	1.45	2.80	59.00	58.81	58.90	1.00	**58.90**	**0.19**
1.83	0.25	1.85	80.57	82.23	81.40	0.99	**74.16**	**71.75**
2.90	1.15	3.15	67.02	68.59	67.80	0.98	**67.80**	**4.99**
1.75	0.35	1.80	76.46	78.79	77.63	0.98	**77.63**	
2.70	0.90	2.80	74.64	71.25	72.95	1.03	**67.40**	
2.93	5.30	6.10	28.65	29.67	29.16	0.98	**27.31**	**27.23**
3.00	5.30	6.00	30.00	27.95	28.98	1.03	**27.15**	**0.12**
3.75	4.10	5.60	42.04	42.93	42.49	0.98	**42.49**	**OUT**
2.33	1.95	3.05	49.67	50.26	49.96	0.99	**49.96**	**51.23**
2.38	1.90	3.10	50.01	52.20	51.10	0.96	**52.51**	**1.80**
1.75	0.40	1.80	76.46	77.16	76.81	0.99	**76.81**	**75.40**
1.80	0.40	1.85	76.65	77.51	77.08	0.99	**77.08**	**3.38**
1.70	0.25	1.75	76.27	81.79	79.03	0.96	**77.36**	
1.78	0.60	1.90	69.10	71.59	70.35	0.97	**70.35**	
2.93	5.00	5.90	29.72	32.06	30.89	0.96	**30.89**	**28.39**
2.83	5.40	6.00	28.09	25.84	26.97	1.03	**25.89**	**3.53**
2.35	1.80	2.95	52.81	52.40	52.60	1.01	**53.36**	**51.81**
3.30	2.70	4.20	51.79	49.99	50.89	1.03	**50.89**	**2.89**
2.13	1.50	2.60	54.82	54.77	54.79	1.00	**54.79**	
3.70	3.30	5.00	47.73	48.70	48.22	0.98	**48.22**	

Table 7.4 - Contact Angles of Substrates with FBS

Left Side

	X	Y	R	arcSin	arcCos	average	Error check
IAG + FBS W	4.75	10.25	11.35	24.74	25.43	25.09	0.99
	3.85	6.00	7.15	32.58	32.95	32.76	0.99
D	5.50	2.75	6.20	62.51	63.67	63.09	0.98
	2.45	0.20	2.50	78.52	85.41	81.97	0.97
F	2.45	0.20	2.50	78.52	85.41	81.97	0.97
IPA + FBS W	3.85	8.10	9.00	25.33	25.84	25.58	0.99
	4.60	11.35	12.20	22.15	21.51	21.83	1.01
D	4.95	2.40	5.45	65.27	63.87	64.57	1.02
	2.50	0.30	2.55	78.64	83.24	80.94	0.98
F	2.50	0.50	2.60	74.06	78.91	76.49	0.96

Right Side

X	Y	R	arcSin	arcCos	average	Error check	Overall Average	average/STDEV
4.75	10.25	11.35	24.74	25.43	25.09	0.99	**25.09**	28.97
3.85	5.95	7.10	32.84	33.07	32.95	1.00	**32.86**	5.50
5.50	2.75	6.20	62.51	63.67	63.09	0.98	**63.09**	OUT photo
2.45	0.20	2.50	78.52	85.41	81.97	0.97	**81.97**	81.97
2.45	0.20	2.50	78.52	85.41	81.97	0.97	**81.97**	81.97
3.85	8.10	9.00	25.33	25.84	25.58	0.99	**25.58**	23.37
4.60	12.60	13.50	19.92	21.04	20.48	0.99	**21.16**	3.13
4.95	2.20	5.40	66.44	65.96	66.20	1.01	**65.38**	Out Photo
2.50	0.10	2.55	78.64	87.75	83.19	0.96	**82.07**	82.07
2.50	0.20	2.55	78.64	85.50	82.07	0.97	**79.28**	79.28

Appendix C – AFM Results

Table 7.5 - AFM Analysis Data

June 8 Anaylsis		
PBS, PBS+FBS, NaCl, NaCl+FBS		
0607-004.tif	JUST PBS	
L=7.266 um		
Rmax=242.4 nm		
Roughness		
On crystals		
Pic	RMS (nm)	RA (nm)
1	8.067	6.436
2	5.844	4.512
3	3.96	3.112
4	4.308	3.304
5	4.377	3.481
STD	1.70170435	1.37801996
Average	5.3112	4.169
On substrate		
Pic	RMS (nm)	RA (nm)
1	3.535	2.623
2	2.251	1.857
3	2.36	1.993
4	3.061	2.607
5	7.393	4.918
STD	2.11937467	1.23440261
Average	3.72	2.7996
0607-009.tif	PBS + FBS	
L=11.250 um		
Rmax=249.86 nm		
Roughness		
On crystals		
Pic	RMS (nm)	RA (nm)
1	33.887	22.386

2	55.656	34.27
3	25.558	20.832
4	23.661	16.555
5	34.429	24.589
STD	12.7014264	6.58625047
Average	34.6382	23.7264
On substrate		
Pic	RMS (nm)	RA (nm)
1	25.248	17.728
2	12.063	9.058
3	14.27	10.619
4	26.564	16.164
5	8.704	6.932
STD	8.05397922	4.64612281
Average	17.3698	12.1002
0607-011.tif	NaCl	
L=3.652 um		
Rmax=6.152 nm		
Roughness		
No Crystals Present		
Pic	RMS (nm)	RA (nm)
1	1.286	0.974
2	1.369	1.069
3	1.381	1.074
4	1.262	1.005
5	1.368	1.107
STD	0.0549427	0.05454081
Average	1.3332	1.0458
0607-014.tif	NaCl + FBS	
L=3.242 um		
Rmax=221.45 nm		
Roughness		
On Crystal	***Structure of long branching X-mas Tree	
Pic	RMS (nm)	RA (nm)
1	16.064	11.919
2	19.928	15.658

3	17.89	14.402
4	21.134	17.415
5	13.678	11.138
STD	2.98487407	2.5998939
Average	17.7388	14.1064
Off Crystal		
Pic	RMS (nm)	RA (nm)
1	4.722	3.843
2	3.351	2.65
3	4.644	3.595
4	2.9	2.404
5	2.306	1.915
STD	1.06935392	0.81383125
Average	3.5846	2.8814
0607-017.tif	NaCl + FBS	
L=6.719 um		
Rmax=53.306 nm		
Roughness		
On Crystal	***Structure of little snowflakes	
Pic	RMS (nm)	RA (nm)
1	24.552	20.325
2	6.941	5.462
3	24.099	18.527
4	8.15	6.646
5	17.982	15.544
STD	8.45210587	6.84502825
Average	16.3448	13.3008
On Substrate		
Pic	RMS (nm)	RA (nm)
1	0.882	0.664
2	1.117	0.831
3	0.862	0.7
4	0.848	0.62
5	1.24	0.987
STD	0.17807358	0.14915194
Average	0.9898	0.7604
0607-020.tif	NaCl +FBS	

L=10.781 um		
Rmax=229.17 nm		
Roughness		
On Crystal	***Structure of little grains	
Pic	RMS (nm)	RA (nm)
1	24.779	20.538
2	29.398	24.659
3	29.982	24.865
4	20.078	15.773
5	20.959	16.54
STD	4.60325023	4.31204574
Average	25.0392	20.475
On Substrate		
Pic	RMS (nm)	RA (nm)
1	2.295	1.894
2	1.266	0.963
3	2.574	2.021
4	2.329	1.885
5	0.994	0.782
STD	0.71006711	0.58702428
Average	1.8916	1.509
0408-048.tif	10% FBS on Gold	
drop		
L=11.016 um		
Rmax=49.413 nm		
On Crystal		
Pic	RMS (nm)	RA (nm)
1	8.051	6.763
2	6.399	5.446
3	6.763	5.465
4	7.235	6.063
5	2.5	1.979
STD	2.15310562	1.84913418
Average	6.1896	5.1432
On Subrate		
Pic	RMS (nm)	RA (nm)
1	0.862	0.65
2	1.297	0.995

3	1.089	0.866
4	1.683	1.427
5	1.149	0.978
STD	0.30437805	0.28367358
Average	1.216	0.9832
0408-036.tif	100% FBS on Gold	
L=1.406 um		
Rmax=160.4 nm		
On Crystal		
Pic	RMS (nm)	RA (nm)
1	17.468	13.703
2	23.359	18.399
3	20.485	16.581
4	16.313	13.279
5	18.013	14.131
STD	2.8136213	2.19163428
Average	19.1276	15.2186
On Substrate		
Pic	RMS (nm)	RA (nm)
1	2.113	1.699
2	2.893	2.276
3	2.493	1.673
4	2.351	1.829
5	4.849	3.949
STD	1.10421339	0.96109999
Average	2.9398	2.2852
0408-031.tif	Just Gold	
L=4.922 um		
Rmax=11.014 nm		
Roughness		
Pic	RMS (nm)	RA (nm)
1	0.487	0.391
2	0.7	0.591
3	0.971	0.746
4	0.66	0.534
5	0.642	0.52
STD	0.17568011	0.12877228
Average	0.692	0.5564

Appendix D – Live/Dead Kit Pictures

(No Picture has been edited. Each photo has an area of 0.158 mm^2.)

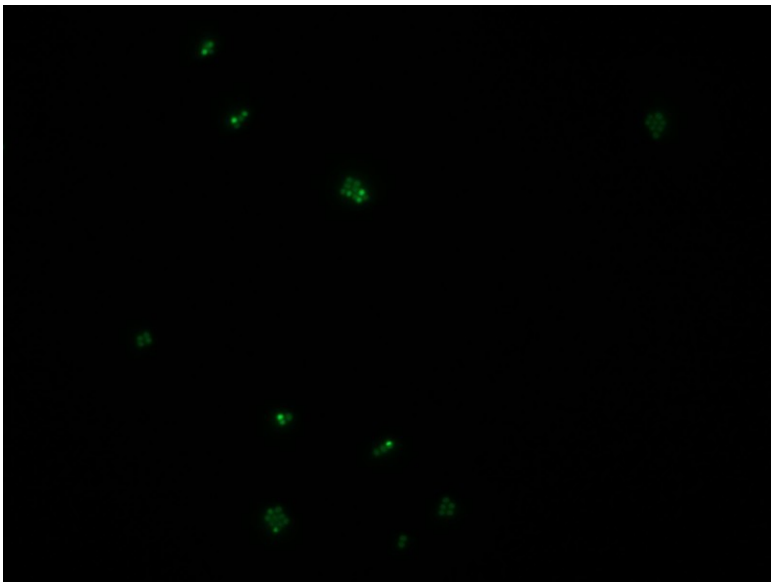

Figure 7.1 – *S. epidermidis* on Gold Viewed Under FITC Filter

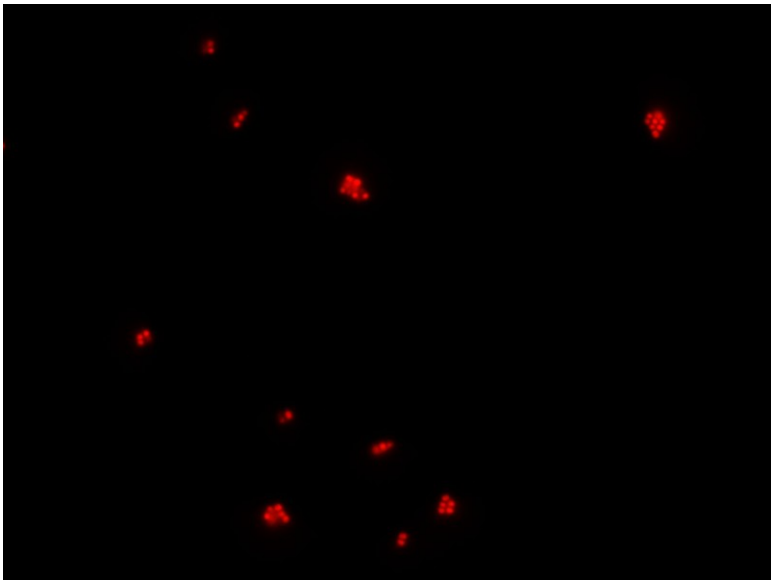

Figure 7.2 – *S. epidermidis* on Gold Viewed Under Texas Red Filter

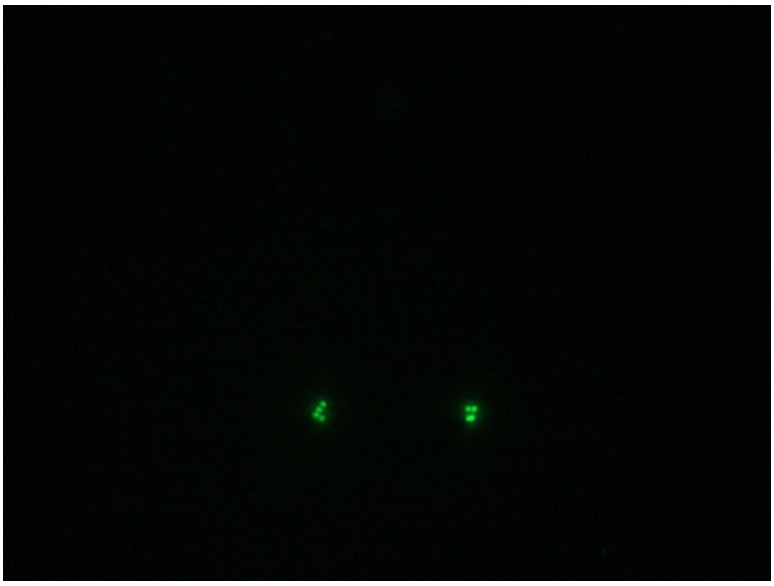

Figure 7.3 - *S. epidermidis* on Glass Viewed Under FITC Filter

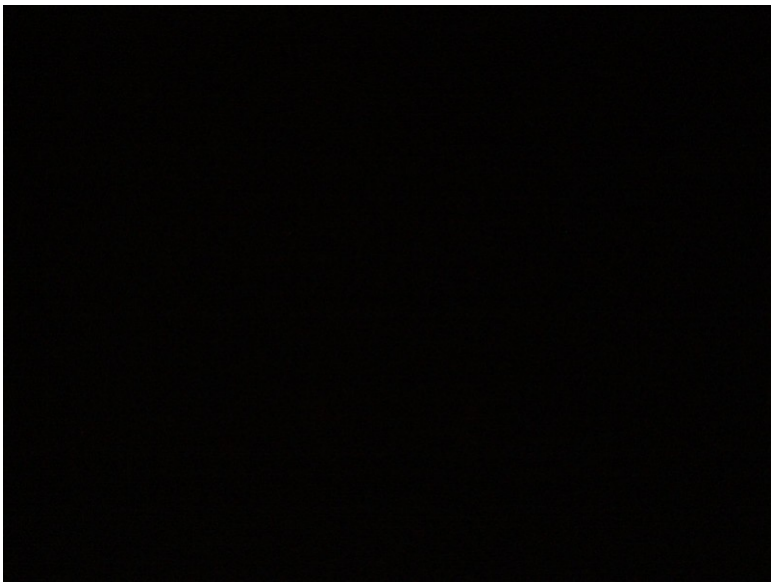

Figure 7.4 - *S. epidermidis* on Glass Viewed Under Texas Red Filter

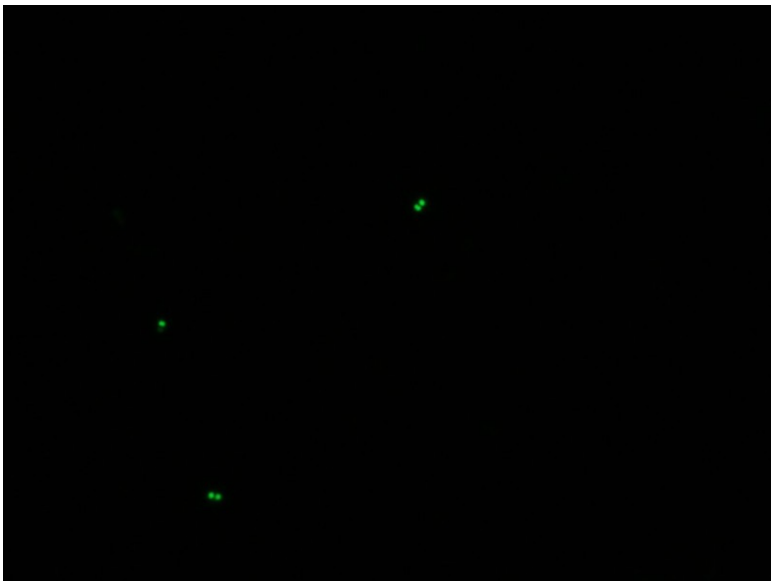

Figure 7.5 - *S. epidermidis* on IPA Viewed Under FITC Filter

Figure 7.6 - *S. epidermidis* on IPA Viewed Under Texas Red Filter

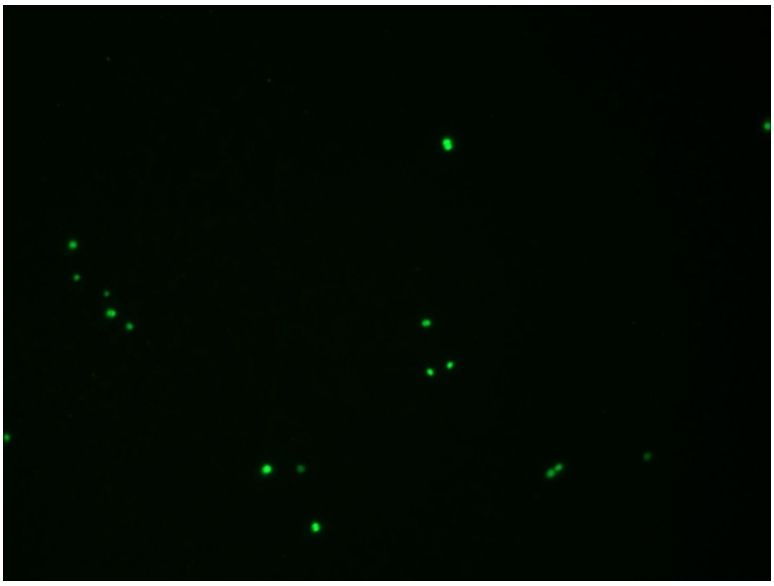

Figure 7.7 - *S. epidermidis* on IAG Viewed Under FITC Filter

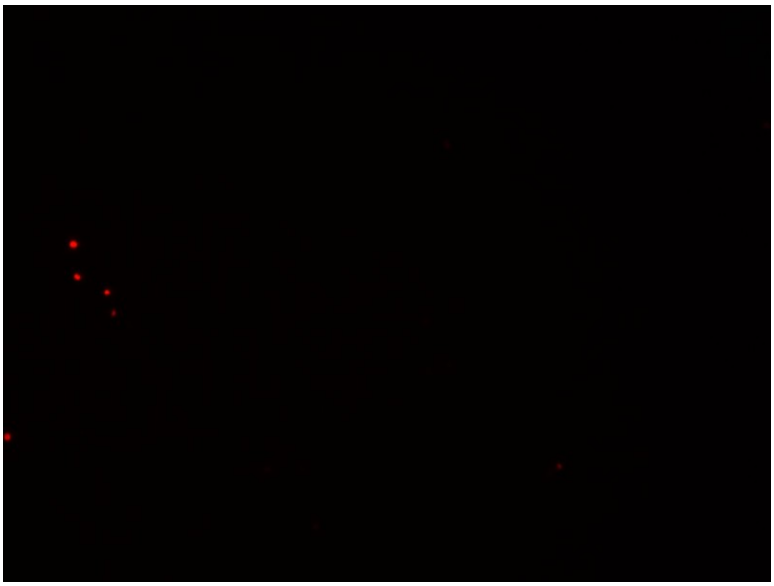

Figure 7.8 - *S. epidermidis* on IAG Viewed Under Texas Red Filter

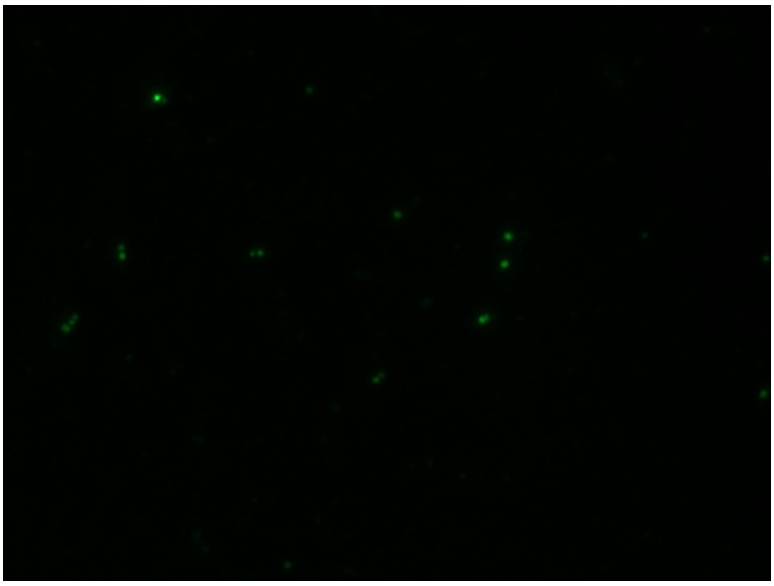

Figure 7.9 - *S. epidermidis* on PYR Viewed Under FITC Filter

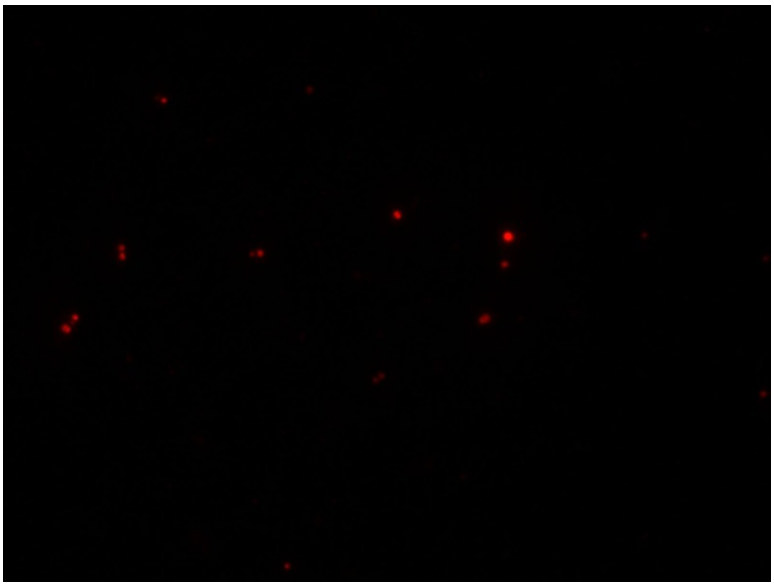

Figure 7.10 - *S. epidermidis* on PYR Viewed Under Texas Red Filter

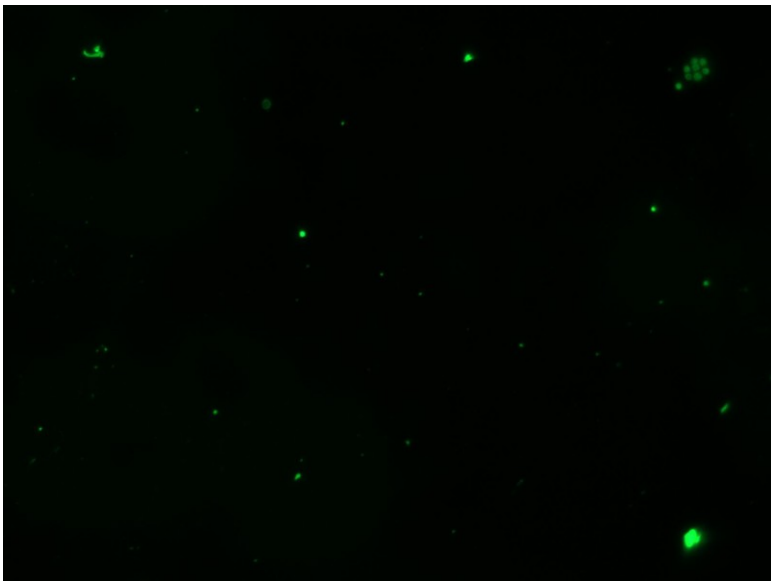

Figure 7.11 - *S. epidermidis* on TEG Viewed Under FITC Filter

Figure 7.12 - *S. epidermidis* on TEG Viewed Under Texas Red Filter

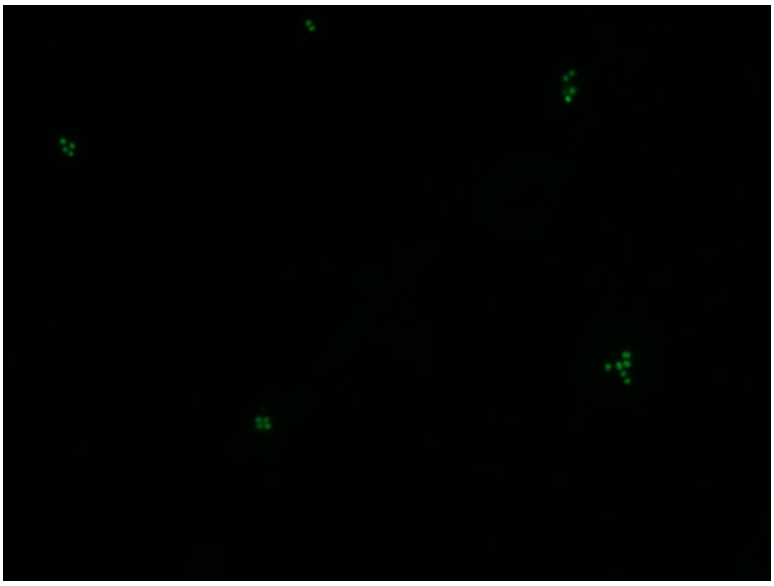

Figure 7.13 - *S. epidermidis* on Gold + FBS Viewed Under FITC Filter

Figure 7.14 - *S. epidermidis* on Gold + FBS Viewed Under Texas Red Filter

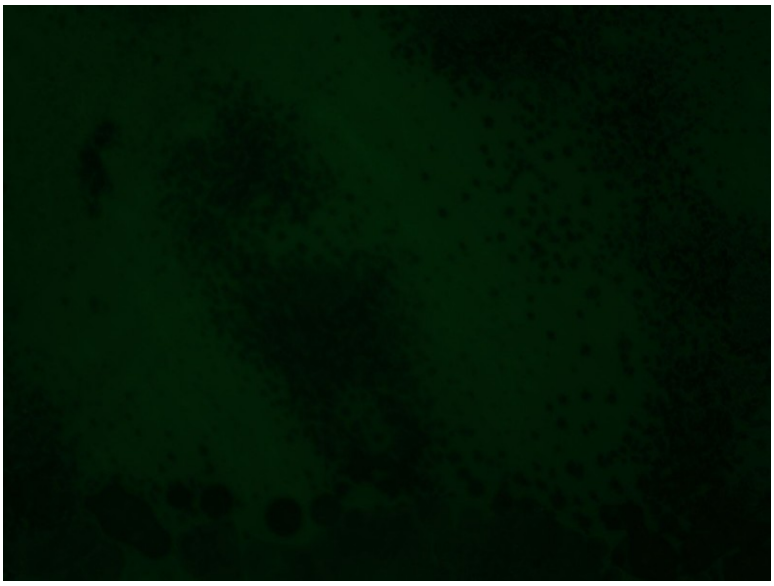

Figure 7.15 - *S. epidermidis* on IAG + FBS Viewed Under FITC Filter

Figure 7.16 - *S. epidermidis* on IAG + FBS Viewed Under Texas Red Filter

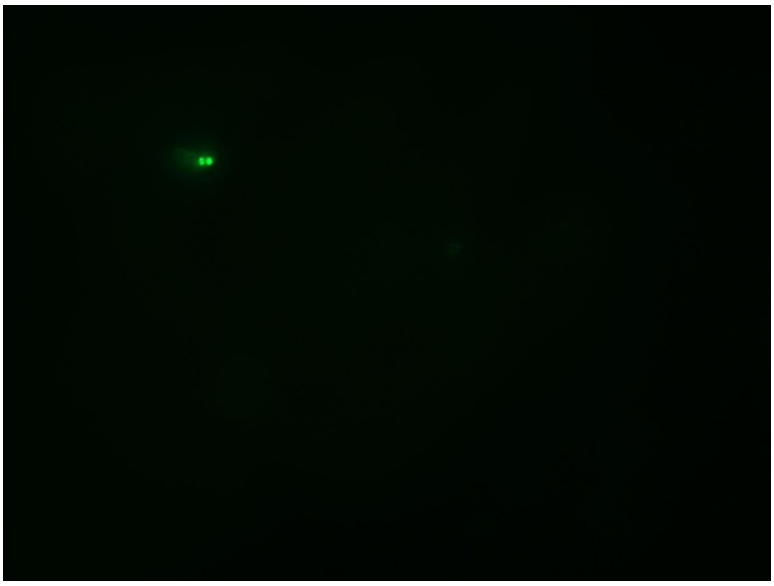

Figure 7.17 - *S. epidermidis* on IPA + FBS Viewed Under FITC Filter

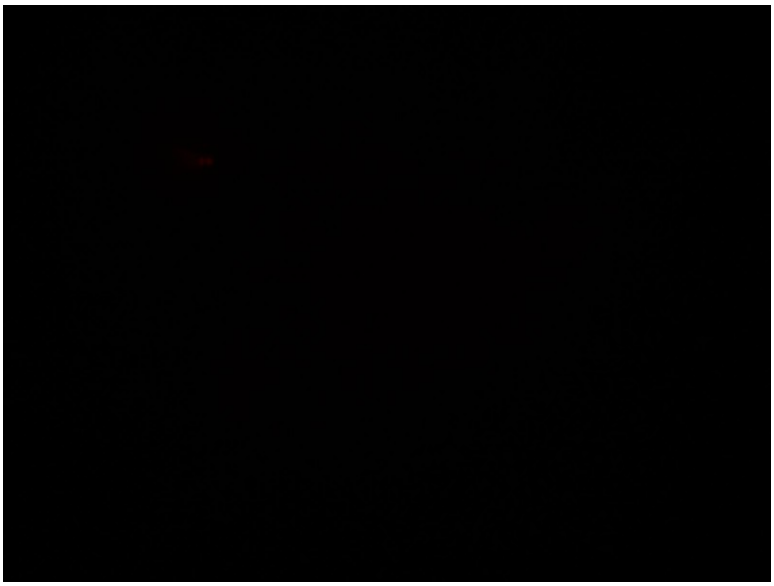

Figure 7.18 - *S. epidermidis* on IPA + FBS Viewed Under Texas Red Filter

Appendix E – Measuring Contact Angles

(Brightness and contrast have been altered with Photoshop)

Figure 7.19 - Example of Formamide Drop on Cleaned Gold

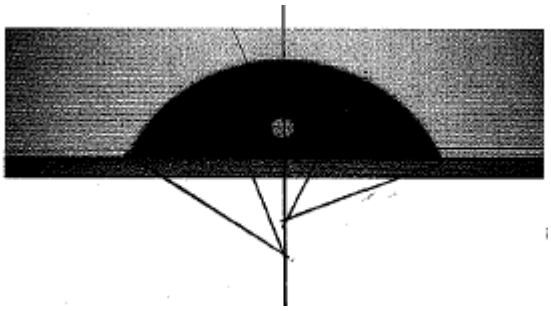

Figure 7.20 – Measuring Contact Angle of Formamide on Uncleaned Gold

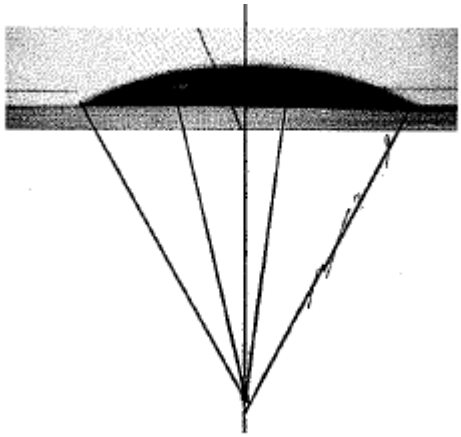

Figure 7.21 – Measuring the Contact Angle of Diiodomethane on Gold

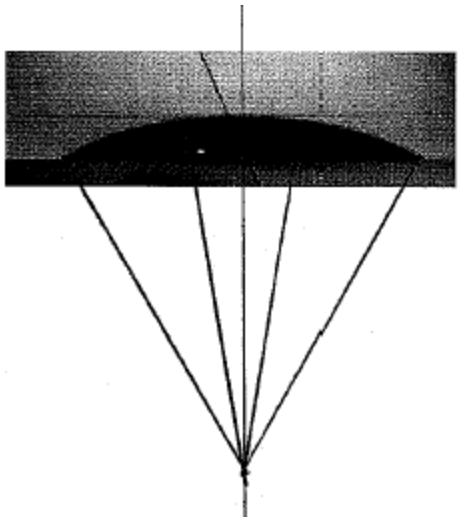

Figure 7.22 – Measuring Contact Angle of Diiodomethane on IAG

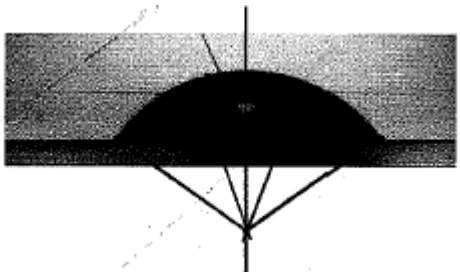

Figure 7.23 – Measuring Contact Angle of Formamide on IAG

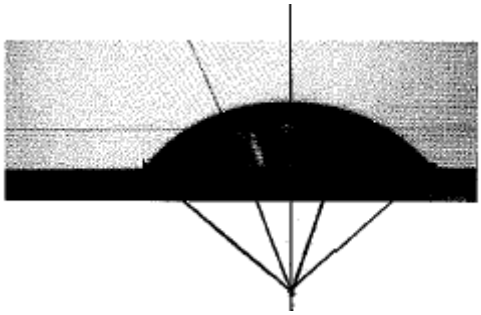

Figure 7.24 – Measuring Contact Angle of Formamide on IPA

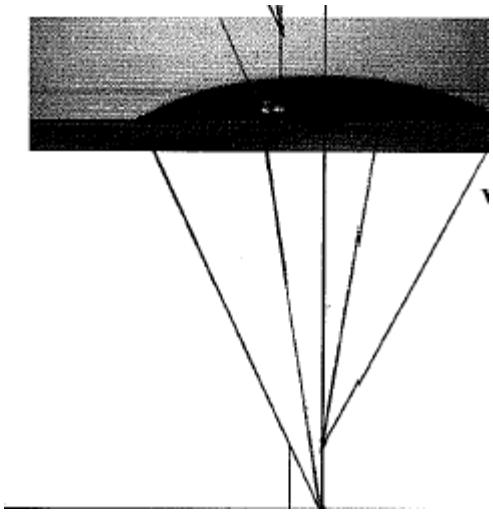

Figure 7.25 – Measuring the Contact Angle of Diiodomethane on IPA

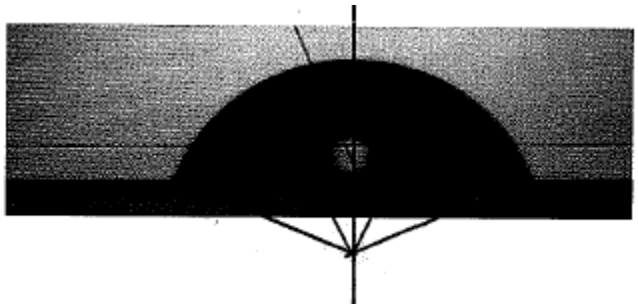

Figure 7.26 – Measuring the Contact Angle of Water on IPA

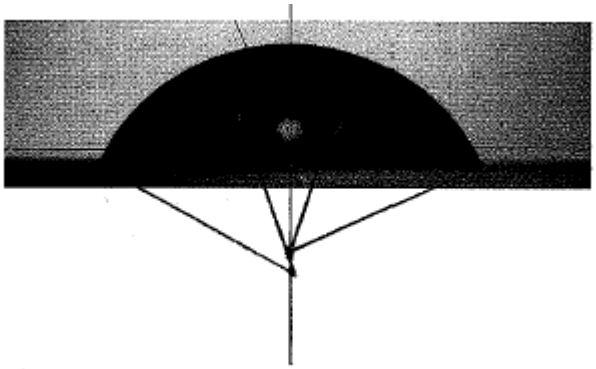

Figure 7.27 – Measuring the Contact Angle of Water on IPA